

Experimental method of stress and strain analysis in biomechanics

R. BĘDZIŃSKI

*Biomedical Engineering and Experimental Mechanics Laboratory
Institute of Machine Design and Operation
Wrocław University of Technology, Poland*

Possibilities of applying several experimental methods to the analysis of displacements, strains and stresses in bone structures and implants are presented. Such methods as: photoelasticity, holographic interferometry, speckle photography and strain gauges are described. These experimental methods are significant nowadays, especially during improvement of modern analytical and numerical methods. Experimental methods are indispensable for experimental verifications of boundary conditions in theoretical models. Experimental investigations of real objects and biomechanical models were carried out.

Key words: photoelasticity, holographic interferometry, speckle photography, ESPI, moiré method, strain gauges.

1. Introduction

The analysis of the stress state of structural components by calculation methods often encounters serious difficulties. The complicated shape, determined chiefly by the constraints imposed by the functions these components have to fulfil, and the complex state of mechanical loads and purely thermal loads are the reasons why results of calculations should be verified through experiments.

Usually, the aim of biomechanical research is the determination of displacement distribution of anatomical samples or physical models. Subjects of investigations are parts of human muscular-skeletal system (bones, joints, ligaments, muscles, other soft-tissues) or orthopaedic implants and devices. For measurements almost all methods of solids mechanics are used. The most popular are strain gauges or testing machines; however, range and importance of optical measurement methods increase nowadays.

Development of modern numerical methods and computational techniques allows to solve highly complex problems encountered in the assessment of the

strength and reliability of bone structures and implants. However, they usually require experimentally determined boundary conditions and description of the involved phenomena. An experimental analysis of tissue structures and implants, which includes empirical activities aimed at determining through experimental analysis the relationships between the quantities that characterise a given object or process, can be divided into three basic stages: the design of an experiment, the realisation of the experiment and the analysis of obtained results. Depending on the goal of an investigation, e.g. the validation of hypotheses, assumptions or mathematical models or the identification of a model of an investigated object, the particular stages of an experiment are subject to modification. The following stages can be distinguished in identification: modelling, an experiment, the estimation of parameters and the validation of the model [1, 3, 11, 12, 13, 17, 31].

Assuming, besides the strength criterion, that the structure should be characterized by specified deformability which would ensure the proper interaction of its members, the use of experimental methods that make it possible to identify the stress state and the state of strains acquires special importance. One should bear in mind that many important practical problems can be solved only through numerical analysis.

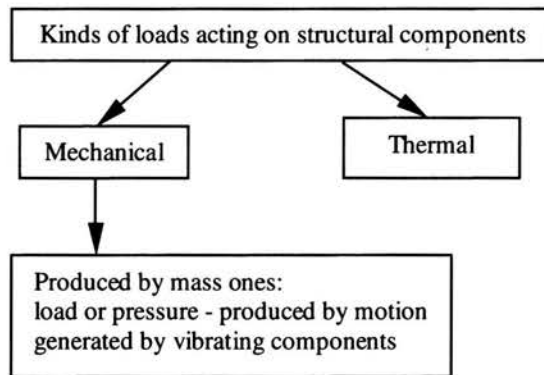


FIGURE 1. The kind of load criterion – a diagram.

The basic kinds of loads shown in Fig. 1 have a steady or dynamic character but as the calculation and research practice shows they are often replaced by static loads. As far as the character of the strains field is concerned, elastic strains are of major importance for practice since the presence of nonelastic strains as a rule disqualifies the structural member in case. The research tasks shown in Fig. 2 can be distinguished in this context. The quoted criteria do not exhaust all stress problems in structural components and deformability

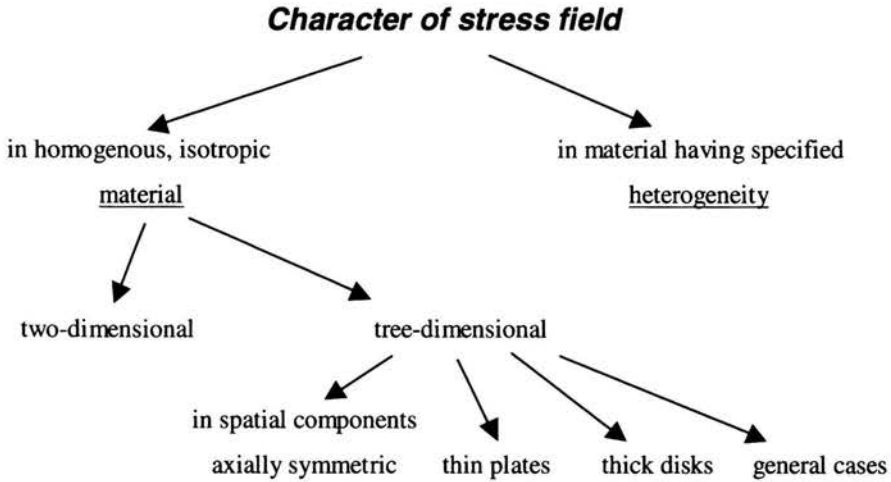


FIGURE 2. Structure of investigation from the point of view of stress field.

problems that occur in practice. For example, problems associated with the preliminary loading of some structural member and with the internal stresses in particular are covered by the criterion shown in Fig. 2, whereas problems of this type are hard to define within the framework of the kind-of-load criterion.

The general aims of studies of components are as follows: to identify stress and deformability states or/and to optimise the studied components according to the adopted optimisation criterion (e.g. strength, weight and so on). These aims must be stated in the terms of a research task's subject. The selection of appropriate research methods and techniques, including the existing limitations such as the available measuring devices, the technical and technological resources necessary to carry out measurement by a particular method, costs, the required accuracy of measurement and the character of the obtained information (e.g. point or surface information), is of the utmost importance for the success of such studies. One should mention here a group of research tasks in which the evaluation of the state of stress or deformability serves the purpose of determining other physical quantities.

Because of large number of limitations the researcher encounters in the measurement practice, the criteria on the basis of which measurement methods are selected are diverse and it is extremely difficult to establish a principle on which this selection should be based. A certain help in the choice of the "optimum" method of measurement may be the knowledge of possible solutions for the particular types of research problems by means of specified methods or measuring techniques.

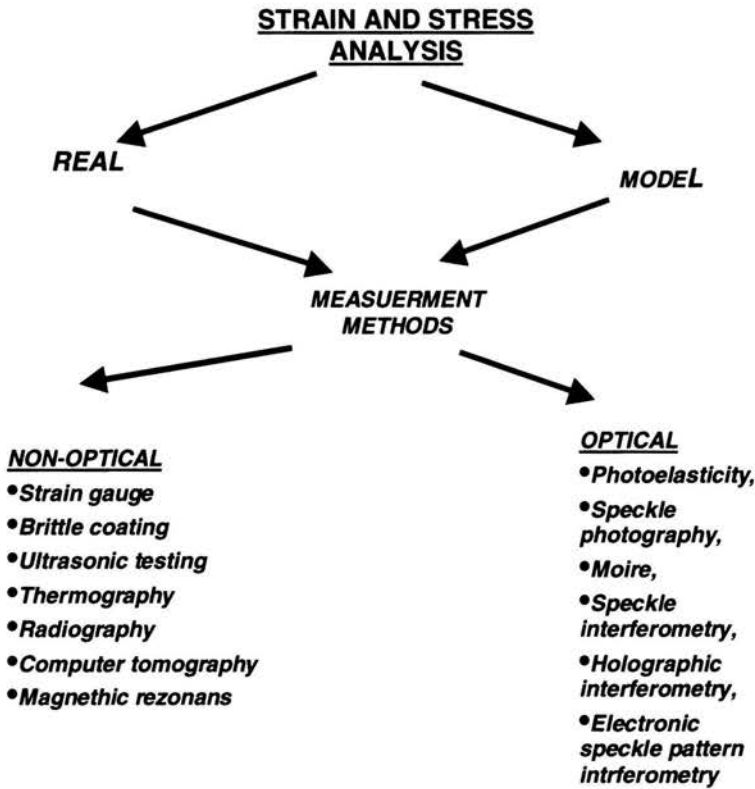


FIGURE 3. Measurement methods.

While the modern analytical methods offer possibilities of solving complex problems not previously accessible to analysis, these solutions are usually based on simplifying assumptions and are calling for an experimental verification. It should not be surprising therefore to see that in parallel with better methods of numerical analysis, the interest in the structural models increased substantially. Some engineers fear that suggestion at a model construction implies lack of competence on their part providing an accurate analysis. In fact, the opposite statement is closer to the true. The component engineering should recognise the application where the model analysis would enhance the reliability and economy of the structure.

The combination of experimental methods with the capacities of modern computers resulted in the creation of tools with almost limitless possibilities in the field of stress and strain analysis [2, 3, 32]. Hybrid techniques (Fig. 4) make it possible to model more accurately and realistically physical processes

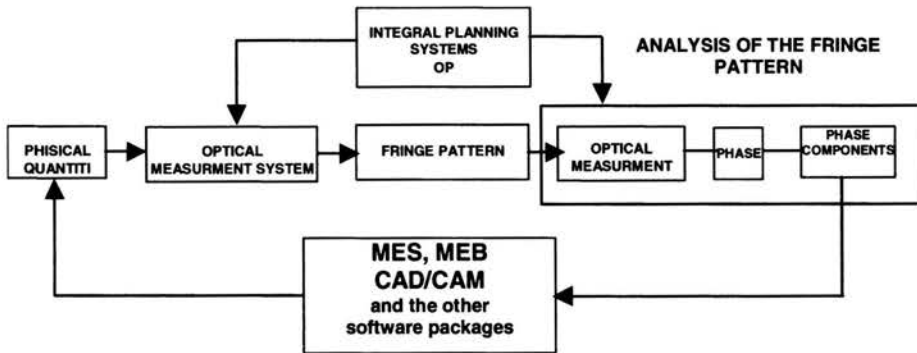


FIGURE 4. An application of the hybrid experimental system in the analysis of stress distribution using optical methods [31, 32].

occurring in biomechanical systems. Such techniques allow to assess the effect of such material properties as heterogeneity and anisotropy, viscoelasticity and viscoplasticity, the variation of stresses and strains in time under loading and macro and micro material constants on the state of stress and strain in bone structures [12].

Methods of experimental investigation of stresses and strains in anatomical parts of the human body have already been established in biomechanical research [1, 5, 7, 10, 14, 37] which in recent years has concentrated on finding out the causes of diseases of man's osteoarticular system and on developing optimal methods of treating them. Usually the most heavily loaded elements such as: the vertebral column, the hip joint and the lower extremities are investigated.

Physical and numerical models should render possibly faithfully a real object and the person conducting an experiment must determine the effect of any simplifications on the obtained results. Generally, it is impossible to model the whole complexity of the ligamentous-muscular system, the nervous system and the biological and biomechanical factors involved in the human osteoarticular system. The analysis of stresses and strains in human anatomical structures and implants by calculation methods often runs into difficulties because of the investigated object's complexity. The complex structure, functions and state of loading are the reason that the adopted calculation models, including numerical ones, must be verified experimentally. If osseous implants are used, it is vital that proper strain and stress relations are maintained in order to ensure the proper interaction between the bone and implant. Experimental methods applied to real objects or their models have become indispensable tools for the identification of such objects.

The methods presented in the present paper are used to identify biomechanical phenomena occurring in bone structures and in implanted endoprostheses and to shape them optimally taking into account limit strength or the maintenance of strains continuity. In this case, designs are evaluated on the basis of stress, strain and displacement distributions determined by various experimental methods. The paper focuses on such methods as photoelasticity, holographic interferometry, interferometry and the electronic speckle interferometry technique, speckle photography, the moiré technique, strain gauges and hybrid methods. The methods enable both the qualitative and quantitative analysis of stresses, strains or displacements in an investigated biomechanical object. Optical measurement methods are particularly useful since measurement here does not involve touching and they offer possibilities of both qualitative and quantitative point and field analysis. The obtained results, related to implant design features, are highly visual. From the beginning it is possible to evaluate the correctness of implants design and thus the whole-investigated field can be analysed. Then by changing the design features of an artificial joint it is possible to obtain optimal, in the designer's opinion, stress or strain distributions. Geometric features of the model can be modified until the sought effect, e.g. a minimal element weight for a uniform distribution of possibly minimum stresses, is achieved.

The considered methods differ in their accuracy. One of the most accurate measurement methods is the holographic interferometry, which allows us to determine displacements in the order of 150-200 nm. Less accurate (by an order of magnitude) is the speckle photography followed by the photoelastic method but the latter allows us to better optimise the shape of implants taking into account the determined stress and strain distributions.

The relative costs of developing and testing a design are an important factor in the selection of design analysis method. The costs of calculation methods should be compared with those of experimental methods, considering the goal to be achieved (Fig. 5). A selection of a research method should also be made on the basis of the relative costs due to the complexity of an investigated object [6].

This paper presents elements of the theoretical basis of optical research methods, especially from the point of view of their application to the experimental analysis of stresses and strains. It focuses on the methods the author followed for many years.

The principles of research by the following methods:

- photo-elasticity,
- holographic interferometry,
- speckle photography,

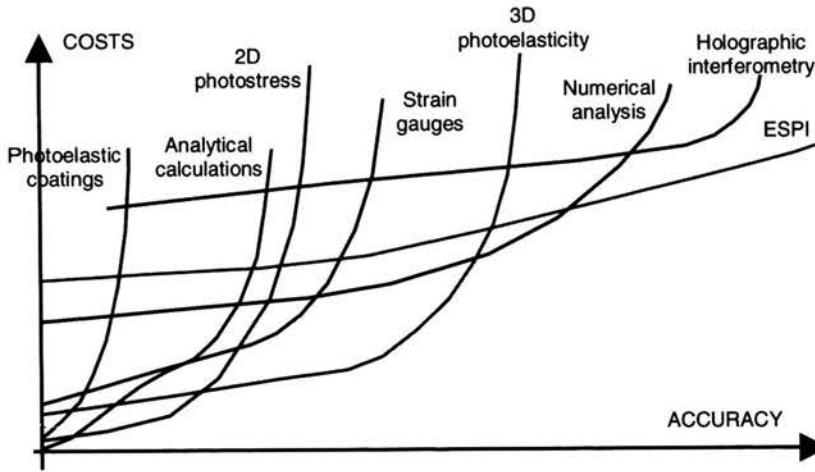


FIGURE 5. Comparison of different experimental methods and numerical analysis from the point of view of total costs as a function of accuracy [12].

- ESPI,
- the moiré effect,
- strain gauge,

are presented and illustrated with examples of the application of optical research methods to the experimental analysis of stresses and strains. Studies of this kind also make possible the quantitative assessment of stress, strain and displacement distributions. Optical measuring methods can be used in studies conducted both on models and on real structures. An additional advantage of these methods is the fact that no touching is involved.

The accuracy of the discussed measuring methods varies. Holographic interferometry, by means of which displacements can be measured with the accuracy of 150-200 nm, belongs to the most precise measuring methods. Speckle photography is by one order of magnitude less accurate. Photoelasticity methods are the least precise but they are the best for the shaping of the machine's members when stress or strain distributions are assessed.

2. Photoelastic methods

The application of the photoelastic methods to studies of two-dimensional models is presented using as an example the optimisation of the shape of the gear pump casing. When shapes were being developed for models of the casing, each time it was assumed that the optimum shape would stem from the condition of boundary stress equalization to a constant value. The method

consists in improving the model initial contour that does not fulfill the constant boundary stress condition by adding or removing material. Changes in the outline determined by photoelastic investigations and an approximate value of the stress gradient reveal a new, corrected shape of the model. This procedure is repeated until the required equalization of stress on the contour is obtained.

2.1. Photoelastic determination of stress distributions in three-dimensional models

The label photoelastic methods [1, 3, 9, 14, 15, 22, 23] and [18] is applied to a set of stress and strain measuring techniques exploiting temporary double refraction which occurs in some materials (e.g. epoxy resins, urethane elastomers, etc). Photoelasticity is usually used to investigate models of real objects but it is possible to make measurements on models in which there is a two- or three-dimensional state of stress. In a full measurement cycle a qualitative and quantitative assessment of the stress distribution in the whole-investigated field can be made, the trajectories of principle stresses can be determined and stress concentrations can be indicated. Photoelastic investigations can be conducted under static and dynamic load conditions. Photoelasticity is the only one experimental method that enables the analysis of a three-dimensional state of stress.

Photoelasticity is used mainly to investigate models of objects and measurements are typically made by shining through the investigated model. Milch (1940) was one of the first researchers who applied photoelasticity to orthopaedics to analyse stresses in the upper part of the femur. Photoelasticity has been applied to investigate stress distributions in models of the spine, hip joint, knee joint and tarsal joint [1, 3, 7, 14, 22, 23].

The photoelastic method of freezing stresses is, apart from the optically sensitive layer method, practically the only method that allows one to analyse three-dimensional states of stress in objects of any shape. The method consists in the fixing, in the model's total volume, of the optical effects produced by a load. This is achieved by loading a model being in a high-elastic state as a results of an elevated temperature, which is then cooled down very slowly. After such freezing of stresses, the model is cut into flat specimens which are then subjected to analysis. The analysis is made on the basis of the obtained polariscope patterns of isoclinic lines and isochromatics. Knowing the isoclinic lines, one can determine the trajectories of principal stresses. The distributions of contour stresses are determined on the basis of isochromatic. Knowing the patterns of isochromatic and isoclinic lines one can separate the components of the state of stress in given section or on the whole surface

of the sample. The number of samples cut out from a model depends on the assumed accuracy of the analysis.

2.2. Course of investigations

Images of isochromatics and isoclinic lines were recorded on photographic plates. To interpret the pictures taken, the following relationship was used [1, 3, 17, 23]:

$$\sigma_1 - \sigma_2 = m \frac{\lambda}{gC} = mK, \quad (2.1)$$

where: m – the isochromatic order, k – photoelastic model constant, σ_1 and σ_2 – principal stresses, C – optical constant, λ – length of light, g – thickness of model.

The value of the stresses on the inside contour of a model of the casing loaded with pressure p was determined by means of relationship (2.2) rearranged to the following form:

$$\sigma_1 = \sigma_K = m \times K \pm \sigma_2, \quad (2.2)$$

where σ_K is the contour stress.

Replacing σ_2 with a value of pressure p which loads the model, the following relation is obtained:

$$\sigma_K = m \times K \pm p, \quad (2.3)$$

which allows one to calculate the stresses on the internal contour of the model (the sign in relationship (2.10) is determined on the basis of stress analysis). The stress on the external boundary of the model are determined by means of relationship (2.4), assuming that $p = 0$:

$$\sigma_1 = \sigma_K = m \times K \pm \sigma_2. \quad (2.4)$$

A loading system should allow one to apply a variable load to the internal contour of the model. The load ought to be zero in the part modelling the suction part and it should have the maximum value in the part representing the pressure part. A structure that fulfils these requirements is shown in Fig. 6. An exemplary picture of full and half isochromatics for model “a” and “b” is presented in Fig. 6.

Contour stress distributions for the studied models were determined on the basis of the obtained distributions of isochromatic lines, using relationships (2.3) and (2.4). A sample distribution of contour stresses for model “b” is shown in Fig. 7.

Contour stress distributions for the studied models were determined on the basis of the obtained distributions of isochromatic lines, using relationships (2.3) and (2.4).

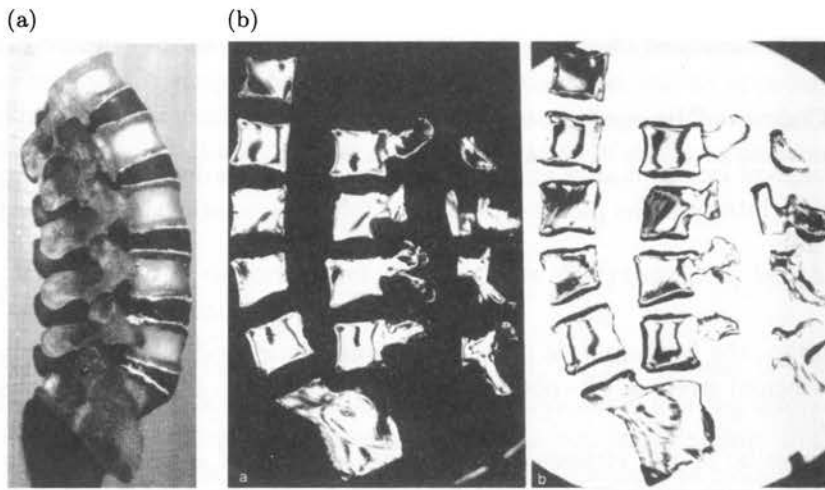


FIGURE 6. (a) Three dimensional model of lumbar spine. (b) An exemplary distributions of full and half - isochromatic pattern in middle slice of lumbar spine [1].

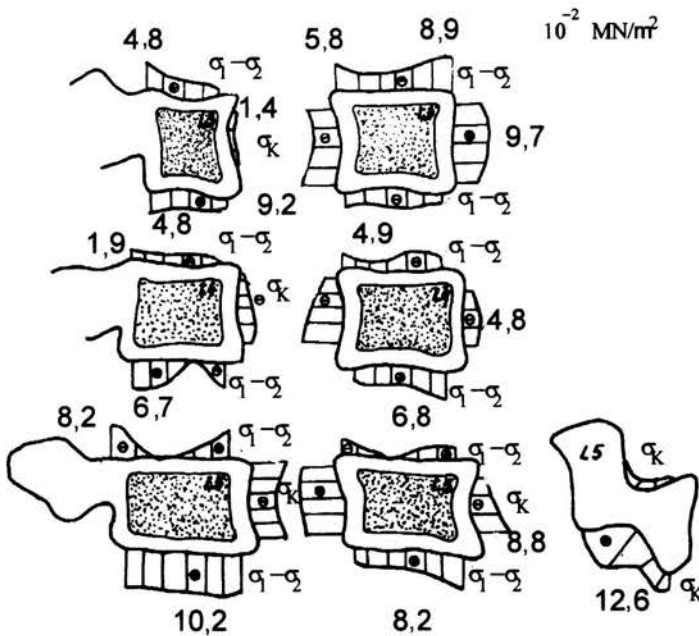


FIGURE 7. Distribution of contour stress and principal stress difference in the selected samples ($\sigma \cdot 10^{-2}$ [MN/m²]).

2.3. Application of photoelasticity in three-dimensional stress analysis in lumbar spine

The vertebral column constitutes the most primary and essential component of human skeletal system and it performs the following three basic functions: protects the spinal cord, serves as the motor system and provides support to the body [1]. The spine, because of its complex and peculiar structure, performs only the first function properly. Performing these multiple functions the spine is subject to considerable loading even in physiological conditions and it is often overloaded. The lumbar part of the spinal column is one of the most important weight – bearing element in human body and plays a crucial role in the carrying of loads. Overloading is a condition in which the physical strength of tissues has been exceeded as a result of the action of forces resulting from the carrying of loads. Degenerative changes caused by overloading include changes in the lower spine, which affect the intervertebral discs, the ligaments and the lateral surfaces of the vertebrae. The mechanism of overload damage to spine elements has not been explained fully yet. The predominant view is that mechanical factors, such as load distributions, the geometry, shape and physical properties of the spine structures as well as stress and strain distributions contribute significantly to the overloading of the spine.

The goal of the investigations presented below was a comparative analysis of three-dimensional state of stress in the lumbar spine under different load conditions. The stress freezing technique was used in the investigations [1, 15]. To match the mechanical properties of the bone better to real conditions, model of lumbar spine consisted of different materials: cortical and spongy bone of the vertebrae was made of epoxy resin, while the disc between vertebrae was modelled by silicon. The spine model was made on a scale of 1:1.

The lumbar part of the spinal column plays a crucial role in the carrying of loads. Degenerative changes caused by overloading include changes in the lower spine which affect the intervertebral discs (discosis), the ligaments (ligamentosis) and the lateral surfaces of the vertebrae (spondylolysis). Spondylolisthesis, often referred to as an overload fatigue syndrome, is a common lumbar spine ailment. The mechanism of overload damage to spine elements has not been explained fully yet. The predominant view is that mechanical factors, such as load distributions, the geometry, shape and physical properties of the spine structures as well as stress and strain distributions contribute greatly to the overloading of the spine. Other factors play also important role, see the paper by Adams in this volume.

2.4. Three-dimensional state of stress in the femur bone

In the alloplasty of the hip joint – the most frequently used implantation (artificial joint) procedure – it is still difficult to choose a suitable endoprosthesis and to evaluate the effects of the operation, especially the short- and long-term probability that the implant will loosen. A predominant view is that the correlation between stresses and strains in the bone and those in the implant (endoprosthesis) determines the success of the reconstruction of the joint [1, 4].

The goal of the investigations presented below was a comparative analysis of the three-dimensional state of stress in the femoral bone and in the same bone with implanted endoprostheses of different types (Aesculap and Autophor). The stress freezing technique was used in the investigations [1, 17, 23]. To match the mechanical properties of the bone and those of the endoprostheses better to real conditions, the models of the two structures were made of different materials based on epoxy resins. The femur bone model and the endoprosthesis models were made on a scale of 1:1. To render the complexity of the state of loading in the hip joint possibly well, a special loading system was constructed. Examples of full isochromatic pattern for sample from the middle part of the three-dimensional models of the femur bone are shown in Fig. 8. Contour stress diagrams for some cross-sections were plotted on the basis of the pattern of the isochromatic lines (Fig. 7). An analysis of the pattern of stresses and isochromatic lines shows clearly that the implanted endoprosthesis (its design) affects the stress pattern significantly [1, 4].

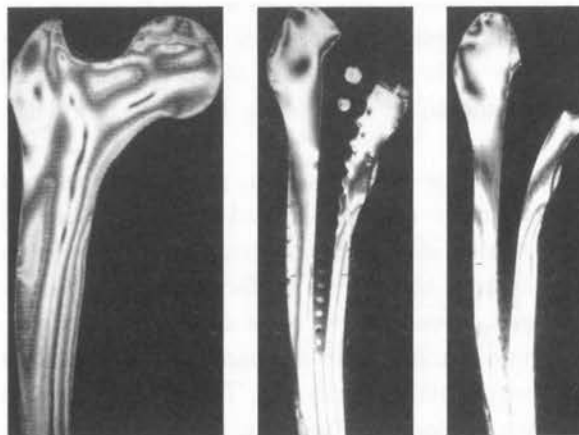


FIGURE 8. Distributions of isochromatics at the model of normal femur and femur with different sort of endoprosthesis stems.

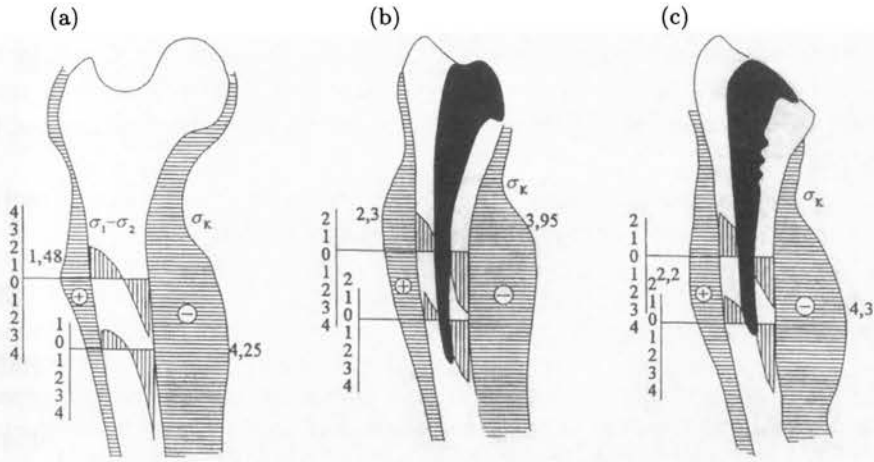


FIGURE 9. Distributions of contour stresses and principle stress difference in longitudinal direction of the model of femur bone: (a) intact bone, (b) bone with P stem, (c) bone with M stem.

3. Photoelastic coating method

The photoelastic coating method has many advantages compared to other methods of experimental stress analysis. It provides point-by-point of full-field quantitative data, enabling the investigator to determine the complete distribution of surface strains and directly highlighting severely strained regions.

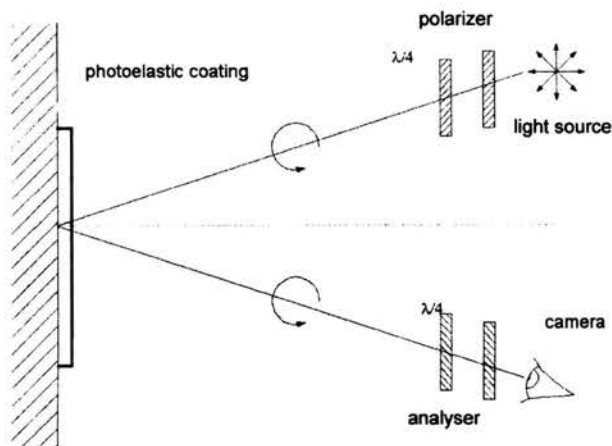


FIGURE 10. Scheme of optical set-up of the photoelastic coating method.

When a photoelastic coating is bonded to a real object, the surface displacements are transmitted to the coating through an adhesive. Consider the case where both the coating and specimen are subjected to a state of plane stress where strains are uniformly distributed through the thickness of the coating (Fig. 10).

Brewster established that: "The relative change in the index of refraction is proportional to the difference of principal strains", or:

$$(n_x - n_y) = K (\varepsilon_x - \varepsilon_y). \quad (3.1)$$

The constant K is called the "strain-optical coefficient" and characterises a physical property of the material. It is a dimensionless constant usually established by calibration and may be considered similar to the "gauge factor" of resistance strain gauges. Combining the expressions above, we have:

$$\delta = tK (\varepsilon_x - \varepsilon_y) \quad (3.2)$$

in transmission, and:

$$\delta = 2tK (\varepsilon_x - \varepsilon_y) \quad (3.3)$$

in reflection (light passes through the plastic twice).

Consequently, the basic relation for strain measurement using the photoelastic coating technique is:

$$(\varepsilon_x - \varepsilon_y) = \frac{\delta}{2tK}. \quad (3.4)$$

Due to the relative retardation δ , the two waves are no longer in phase when emerging from the plastic. The analyser A will transmit only one component of each of these waves (that parallel to A). These waves will interfere and the resulting light intensity will be a function of:

- the retardation δ ,
- the angle between the analyser and direction of principal strains ($\beta - \alpha$).

The fringe orders observed in photoelastic coatings are proportional to the difference between the principal strains in the coating (and in the surface of the test part). This simple linear relationship is expressed as follows

$$\varepsilon_x - \varepsilon_y = Nf, \quad (3.5)$$

where:

$\varepsilon_x, \varepsilon_y$ - principal strains,

N - fringe order,

$f = \lambda/(2tK)$ - fringe value of coating,

λ – wavelength (in white light $22.7 \cdot 10^{-6}$ inches or 575 nm),
 t – thickness of coating,
 K – stress optical coefficient of coating.

Equation (3.5) can also be written in terms of shear strain, γ_{xy} :

$$\gamma_{xy} = Nf, \quad (3.6)$$

where γ_{xy} is maximum shear strain (in the plane of the part surface) at any point.

The significance of the preceding is that the difference in the principal strains, or the maximum shear strain in the surface of the test part, can be obtained by simply recognizing the fringe order and multiplying by the fringe value of the coating.

Engineers and designers often work with stress rather than strain; and, for this purpose, Eqs. (3.5) and (3.6) can be transformed by introducing Hooke's law for the biaxial stress state in mechanically isotropic materials:

Relative liner phase difference for a coating thickness has the form

$$R = wtC(\sigma_{1c} - \sigma_{2c}) \quad (3.7)$$

where:

R – relative retardation,
 t – thickness of coating,
 C – stress-optic coefficients,
 σ_{1c}, σ_{2c} – principal stresses in the coating.

Equation (3.7) expresses the stress-optic law as it is commonly applied in photoelasticity (reflection method). This could be expected since from Eq. (3.7) we have:

$$\sigma_{1c} - \sigma_{2c} = \frac{R}{2tC} = \frac{m\lambda}{2tC} = m\frac{K}{2}, \quad (3.8)$$

where:

m – order of the isochromatic pattern,
 λ – wavelength,
 K – stress optical coefficient of coating.

The relations between the stresses and strains in the coating are:

$$\begin{aligned}\sigma_{1c} &= \frac{1}{E_c} (\varepsilon_{1c} - \nu_c \varepsilon_{2c}), \\ \sigma_{2c} &= \frac{1}{E_c} (\varepsilon_{2c} - \nu_c \varepsilon_{1c}), \\ \sigma_{3c} &= 0, \\ \sigma_{1c} - \sigma_{2c} &= \frac{E_c}{1 + \nu_c} (\varepsilon_{1c} - \varepsilon_{2c}),\end{aligned}\tag{3.9}$$

where:

E_w – modulus of elasticity of the coating,

ν_w – Poisson ratio,

$\varepsilon_{1c}, \varepsilon_{2c}$ – strain of coating,

σ_{1c}, σ_{2c} – stress in the coating.

We have

$$\varepsilon_{1c} - \varepsilon_{2c} = \frac{1 + \nu_c}{E_c} m \frac{K}{2}.\tag{3.10}$$

The strains in the coating are equal: $\varepsilon_{1c} = \varepsilon_{1o}$ and $\varepsilon_{2c} = \varepsilon_{2o}$; moreover

$$\varepsilon_{1o} - \varepsilon_{2o} = \frac{1 + \nu_c}{E_c} m \frac{K}{2}, \quad \varepsilon_{1o} - \varepsilon_{2o} = \frac{1 + \nu_o}{E_o} (\sigma_{1o} - \sigma_{2o}).\tag{3.11}$$

Thus the stresses in the coating are linearly related to the stresses in real object. With the elastic constants (E, ν) of both materials entering into the proportionality coefficient, we get

$$\sigma_{1o} - \sigma_{2o} = \frac{1 + \nu_c}{1 + \nu_o} \frac{E_o}{E_c} m \frac{K}{2}, \quad f = \frac{1 + \nu_c}{1 + \nu_o} \frac{E_o}{E_c} \frac{K}{2},\tag{3.12}$$

$$\sigma_{1o} - \sigma_{2o} = mf,\tag{3.13}$$

where:

f – optical and material constant,

σ_{1o}, σ_{2o} – principal stress in the object,

$\varepsilon_{1o}, \varepsilon_{2o}$ – strain of coating.

The optical response of a photoelastic coating to the stress field in a coated object can be evaluated by defining a stress – sensitivity index S_σ as follows

$$S_\sigma = \frac{N}{\sigma_{1o} - \sigma_{2o}},\tag{3.14}$$

where N is an integer also called fringe order.

3.1. Applications of photoelastic coating

The photoelastic [1, 9, 14, 17] coating is the most versatile method, which provides full - field strain measurements on real structures under different loads conditions, e.g., static and dynamic. Typically, optically sensitive material is applied onto the surface of an object made of the original material. This particular experimental method is suitable for laboratory or field measurements, using lightweight portable equipment. It is possible to make measurements in such a way that a ray of polarised light passes through a layer of optically sensitive material twice (the reflected light technique). Using that method it is possible to provide for observation and measurement of assembly stresses as mating components are joined. Besides the residual stresses residing in a material as a result of the manufacturing process can be detected. Photoelastic coating is useful in detecting yielding, since any permanent deformations that occur in the part or structure will be displayed in the coating after removal of the test forces.

The photoelastic coating method has many advantages compared to other methods of experimental stress analysis. It provides point-by-point of full-field quantitative data, enabling the investigator to determine the complete distribution of surface strains and directly highlighting severely strained areas.

When a photoelastic coating is bonded to a real object, the surface displacements are transmitted to the coating through the adhesive. Consider that both the coating and the specimen are subjected to a state of plane

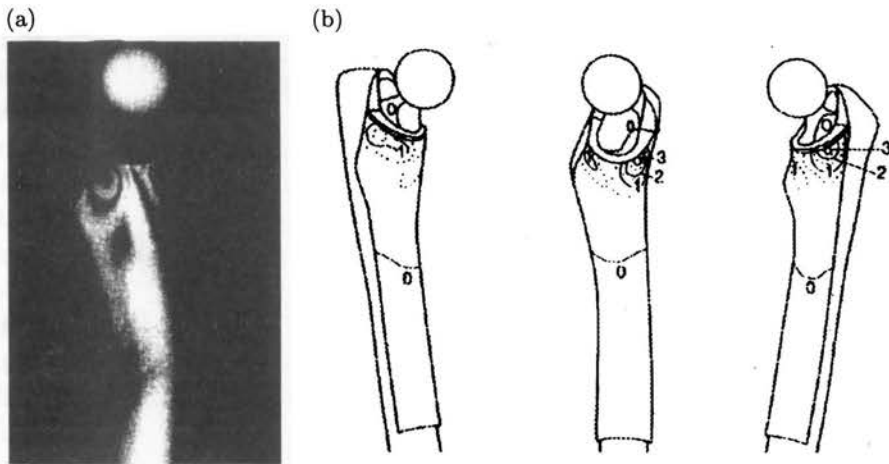


FIGURE 11. Femur bone with the photoelastic layer: (a) isochromatics pattern, (b) distributions of the isochromatics in different parts of bone [14].

stress where strains are uniformly distributed through the thickness of the coating (Fig. 10).

This optical method has been successfully used in biomechanical research for the past 30 years. A typical example of practical application of the photoelastic coating is shown in Fig. 11.

4. Application of holographic interferometry

Holographic interferometry combines the measurement of small displacements with holographic image recording. At the moment this method ensures the highest sensitivity of measurement, it is universally applicable and it enables both the qualitative and quantitative analysis of whole investigated fields (even large ones). Another advantage is that measurements can be made on the real object without touching it [1, 4, 6, 7, 9, 15, 16, 17, 20, 23, 32].

Holographic interferometry is based on the principle of double recording of the image of an investigated object and it is used to measure small displacements of points on the surface of a body subjected to all kinds of loads, e.g. mechanical loads, thermal loads, vibrations, or to study mechanisms of failure of structural elements. The obtained information about the displacement of the investigated object's surface is used to calculate stress and strain values by differentiating the displacement field and taking into account the physical properties of an investigated object.

Holographic interferometry is a method of measuring displacement that is based on the principles of the holographic recording of the studied object's image. The method is used for measuring small displacement of points on the surface of a body subjected to mechanical, thermal and other loads, for analysing vibrations, tracking mechanisms of the destruction of composite materials' structure and so on. The obtained information on the displacements allows one to determine the strains and the stresses by differentiating the field of displacements and also can be used for the non-destructive control of the correctness of execution of e.g. mechanical or biomechanical objects.

Generally speaking, holography is a method of recording amplitude and phase information about an object illuminated by a beam of coherent light on proper light-sensitive material. In the traditional photography, we deal with a one-stage process of fixing a picture, which has an exclusively amplitude character (the distribution of light intensity). Whereas holography is characterized by two stages, i.e. that a recording, during which amplitude-phase information on the recorded wave front. A typical optical system which allows one to record and reproduce a hologram is shown in Fig. 12. Monochromatic

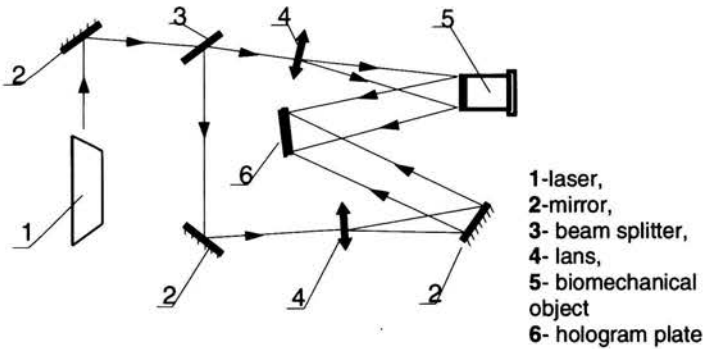


FIGURE 12. Scheme of optical set-up of the holography interferometry.

coherent light emitted by a laser is divided by the so called beam divider into an object beam and a reference beam. The former beam formed suitably by mirrors and the lens illuminates an object and then some of the scattered light reaches a plate covered with a layer of light-sensitive material. The latter one (reference) is directed so that when it falls on plate covered with the recording material it carries information about the source of the light. As a result of the interference of the wave fronts of the two beams, an arrangement of interference spectral lines forms in the plane of recording, which is not visible to the naked eye (the inter-line spacing is about $5 \cdot 10^{-4}$ mm). After the chemical treatment of the plate covered with light-sensitive emulsion (hologram), the stage of the reproduction of the recorded image takes place. This consists in the illumination of the hologram with the reference beam, and at same time it is possible to observe a virtual image or the real one during reconstruction, the reproducing beam diffracts into a hologram (similarly as in the case of the phenomena that occur on a conventional diffraction grating) which transforms the deformed wave front. As a result, when the beam passes through a hologram it carries all the information about the object recorded during the recording stage. In particular, information of phase nature is reproduced whereby it is possible to observe a three-dimensional image of the object. It should be noticed that no optical system converting the image of the examined object is needed for the recording of a hologram.

Holographic interferometry is a kind of holography in which one of the following recording techniques is used during the taking of the so called interferogram (i.e. during the stage of the recording of an examined object):

- Double exposure – two holograms of an object in two different states (e.g. prior to and after the loading with a force, a pressure and so on) are recorded on the same plate before it is subjected to chemical treatment;

- Real time – after chemical treatment, a hologram of an object in the “zero” state is placed precisely in the position corresponding to the recording and then the object is observed through the hologram.
- Time average single hologram of an object subjected to cyclical changes in the shape of its surface (e.g. vibrations) is produced; in this case, the difference in the contrast of the images of these surface points which undergo substantial and very small displacement is utilised.

In all the cases, two or more three-dimensional images of an object formed closely to one another in space are reproduced simultaneously during the reconstruction of a holographic interferogram. These, by interfering with each other, form a system of dark and light spectral lines visible against the background of the object. The spectral lines run through points having the same value of displacement along the observation axis.

4.1. Double exposure technique

Let us denote functions describing the two wave fronts of the object beam (during the first and the second exposure, respectively) by U_{01} and U_{02} and the wave front of the reference beam by U_r . It is known that light-sensitive material is a detector of the averaged energy of light incident during an exposure. Thus the distribution of light intensity fixed in an interferogram is described by this formula:

$$I = |U_{01}|^2 + |U_{02}|^2 + |U_r|^2 + U_r^*(U_{01} + U_{02}) + U_r(U_{01}^* + U_{02}^*), \quad (4.1)$$

where star denotes complex conjugates.

Let

$$U_{01} = A_0 \exp iK\phi_{01}, \quad U_{02} = A_0 \exp iK\phi_{02}, \quad (4.2)$$

$$U_r = A_r \exp i \left[K \left(r \sin \alpha + \frac{r^2}{2Z} \right) \right],$$

where:

$k = 2\pi/\lambda$ – the wave number,

ϕ_0 – the reference beam’s phase,

A_{0r} – the amplitude,

r – the wave front’s curvature,

Z – the distance between the light source and the plane of recording,

α' – the angle between the plane of recording and the direction of incidence of the reference beam.

During the reproduction of an interferogram a wave front will be produced as a result of the superimposition of fronts $U_{01} + U_{02}$, with the intensity of light

in the reproduced image being a function modulated by a factor associated with the object's deformations $\phi_{02} - \phi_{01}$:

$$I = 2 |A_0|^2 \{1 + \cos [K(\phi_{02} - \phi_{01})]\}. \quad (4.3)$$

Relationship (4.3) can be simplified if it is assumed that direction of displacement z_1 of the object's surface point is perpendicular to this surface. If the angle of incidence of the reference beam (measured relative to the normal to the object's surface during recording) is denoted by α and the angle of observation (measured relative to the normal to the surface during reconstruction) by β , then the intensity of light in the observed image will be:

$$I = 2 |A_0|^2 \{1 + \cos [kz, (\cos \alpha + \cos \beta)]\}, \quad (4.4)$$

and then the identity $\cos^2(x/2) = (1 + \cos x)/2$ is taken into account:

$$I_p = 4 |A_0|^2 \cos^2 \frac{1}{2} [kz_1 (\cos \alpha + \cos \beta)]. \quad (4.5)$$

The above relationship describes the position of interferogram spectral lines on surface of the object's image. The intensity of illumination changes with the square of the cosine between the spectral lines corresponding to deformations z_1 . by introducing the notion of the spectral line's order N , relationship (4.5) can be written in a form which allows one to determinate directly displacement z_1 :

$$z_1 = \frac{N\lambda}{\cos \alpha + \cos \beta}. \quad (4.6)$$

In practice, this relationship for $\alpha, \beta \approx 0^\circ$ assumes the form $z_1 = N\lambda/2$.

4.2. Real time technique

When this measurement technique is used, the hologram is illuminated by a reference beam identical with the one used in the process of its recording. The reconstructed image is projected onto the real object whose illumination has not changed. Assuming that for static displacements the state corresponding to the recording of a hologram is characterized by displacement $z_2 = 0$, the intensity is describe by an identical relation as (4.5). In the general case, however, the object may be subjected simultaneously to a static load and a changing load (e.g. harmonic vibration). Then wave front U_{cr} (being a vector sum of the reproduced front and the front corresponding to the current state of the object) is described by the following function:

$$U_{or} = A_0 + A_0 \exp(ik\gamma z_1 + ik\gamma z_2 \omega t), \quad (4.7)$$

where:

γ – the function of the angle of incidence of the object beam on the object and of the observation angle,

z_1 – the static displacement of the object,

$z_2 \cos \omega t$ – the displacement caused by vibrations of frequency ω and amplitude z_2 .

The intensity of light is then given by this relation:

$$J_{or} = z |A_0|^2 \{1 + \cos [K z_1 (\cos \alpha + \cos \beta)] J_0 [K z_2 (\cos \alpha + \cos \beta)]\}, \quad (4.8)$$

where: J_0 – Bessel's function of the first kind of zero order. In particular, for $z_1 = 0$:

$$J_{or} = 2 |A_0|^2 \{1 + J_0 [k x_2 (\cos \alpha + \cos \beta)]\}. \quad (4.9)$$

In practice, the effect of function J_0 manifest itself in the considerably reduced contrast of the spectral lines observed during measurement.

4.3. Time average technique

This technique uses the image recorded during a single exposure the duration of which is long in comparison with the vibration period. Therefore, the hologram allows one to reproduce the images of the object's surface in all the positions which occurred during the exposure. During the reconstruction of such a set of images their interference will take place and the observed spectral lines will correspond to the deformations of the examined surface. The light intensity in such a case is described by the following relation:

$$J_{uc} = |A_0|^2 \left[\frac{1}{2} \int_0^T \exp(ik\gamma z_2 \cos \omega t) dt \right]^2, \quad (4.10)$$

where T is the vibration period.

The above relation can be simplified considering that:

$$J(x) = \frac{i^{-n}}{2\pi} \int_0^{2\pi} \exp(ix \cos t) \exp(int) dt. \quad (4.11)$$

For $n = 0$:

$$I_{uc} = |A|^2 J_0^2 [k\gamma z_{12}]. \quad (4.12)$$

After the expansion of function γ , the following is obtained:

$$I_{uc} = |A_0|^2 J_0^2 [k(\cos \alpha + \cos \beta) u_2]. \quad (4.13)$$

Intensity (4.12) is modulated by J_0^2 and it reaches the maximum when the argument of function J_0 is equal to zero. Therefore if $z_2 = 0$, light intensity in the reconstructed image is the strongest. In other words, the object's surface points with intensity $I_{uo} = I_{\max}$ correspond to the vibration to the analysis of polyharmonic vibrations and even transients.

4.4. Sources of coherent light

In measurements by the holographic interferometry method, light sources peculiar for holography-lasers (Light Amplification by Stimulated Emission of Modulation) – are used. In the general case, the interference spectral lines observed in the interferogram carry information only about displacement component δ (Fig. 12):

$$\delta = (\vec{k}_1 - \vec{k}_2)\vec{d}. \quad (4.14)$$

This means that if the bisector of the angle between the illumination direction and the observation is close to the normal of the object's surface, then only displacement component d can be determined:

$$d = \frac{N\lambda}{2 \cos \phi}, \quad (4.15)$$

where: $\phi = \frac{1}{2}(\alpha + \beta)$.

To determine all the three components of the displacement vector (in the Cartesian co-ordinate system), one should use a measuring system similar to that shown in Fig. 13. A beam of coherent light is divided in such a way as to make it possible to record simultaneously three holograms placed not in one

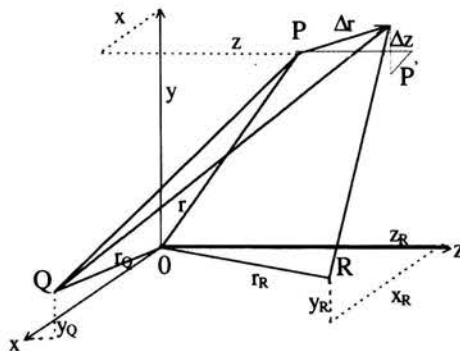


FIGURE 13. Co-ordinate system for analysis of interferograms. Q – position of light source, R – observation point, P – investigated point on object, P' – point on object after displacement.

plane. An analysis of the displacement vector component in the direction is carried out for each hologram.

The determined component has the form:

$$d_i = N_i \frac{\lambda}{2 \cos \phi_i} \quad (i = 1, 2, 3) \quad (4.16)$$

together with the information on the directions allows one to calculate the vector \vec{d} .

4.5. Application of holographic interferometry in the displacements vertebrae analysis

Loads acting on the vertebral body, the intervertebral junctions and the ligamentous-muscular elements contribute largely to deformities and dysfunction of the spine. The spine under such loads assumes an appropriate shape affecting the spine's curvatures, e.g. in the sagittal plane. The analysis of stresses, strains and displacements of the vertebra's elements in spondylopathy induced by overloading may shed some light on the pathological mechanism. In recent years holographic interferometry has been increasingly used to analyse deformations of bone elements [1, 3].

The aim of this research was to study the deformation of the vertebral arch of the lumbar spine in load conditions which modelled the motor activity. As it is known, under overload the isthmus often breaks and as a result a vertebra may slide (spondylolisthesis). The object of the study was real lumbar vertebra L5 prepared from a cadaver. The loads acting on the vertebral arch as a result of the spine's motion in the sagittal plane (Fig. 14) were modelled.

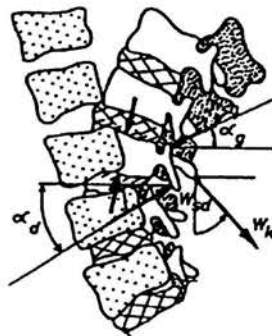


FIGURE 14. The loads acting on the vertebral arch as a result of the spine's motion in the sagittal plane.

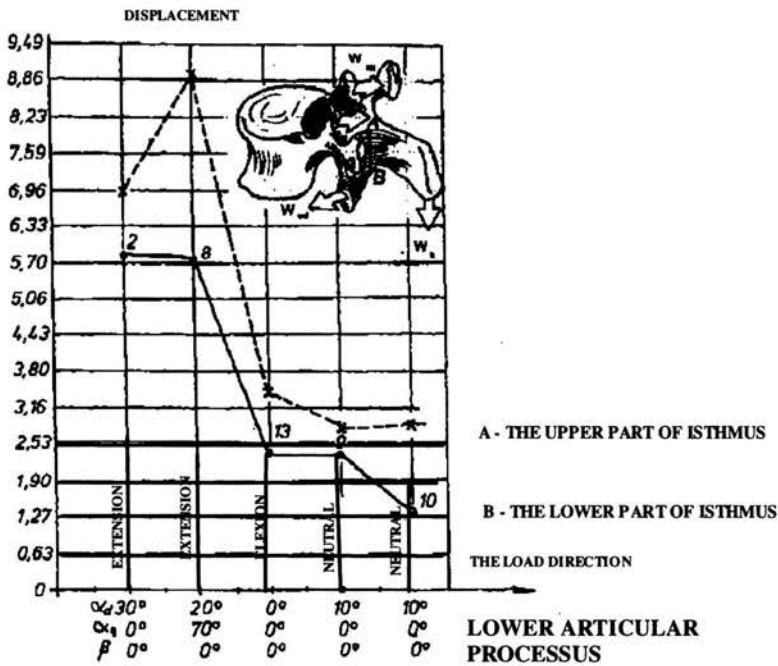


FIGURE 15. Displacement distribution at isthmus of lumbar vertebra under different load conditions.

Changes in the displacement of upper A and lower B points on the pedicle for vertebra L5 for different actions of the spine are shown in Fig. 15. It has been demonstrated that the actions (extension, flexion, hyperextension) affect significantly the distribution of pedicle displacements. Changes in the curvature of the spine have a marked influence on the values and directions of the displacement of the vertebral arch's elements. The recorded considerable gradients of the displacements of some points on the pedicle for the bend-hyperextension movement indicate that the pedicle may be overloaded, especially when the action is performed in the whole range of movement.

Stress and stress distributions in the vertebral arch, particularly in the pedicle, were analysed. The loads acting on the spinous process were determined by means of the Stotte model [1]. Holographic interferometry was used as the test method [17].

4.6. Strain tensor of human lumbar vertebrae

The developed research methodology involving the determination of three displacement components by means of the holographic interferometry tech-

nique makes it possible to determine very small values of displacement and stress components. The methodology can be applied to the investigation of real objects, i.e. vertebra cadaver specimens. Three-dimensional holographic interferometry is particularly suitable for biomechanical studies since the displacement of a real object is measured and the measurement does not involve touching. The method can be used to determine the tensor of strain or stress of complex objects such as bone with implants. Consequently, the proposed method is especially useful in analysing small biomechanical elements, strained in a complex way like vertebrae, arm and lower extremities. The high cost of experiments, difficulties in adjusting the system are the main disadvantages of this particular optical method.

The strain and stress distributions in the vertebral arch vary significantly depending on the applied scheme of loading. Thus one can say that the vertebral arch clearly responds to the function of the vertebra performs and to the kind of loading. Because of the complex structure of the vertebra (sharp variations in its cross-section and mechanical properties), the strain and stress distributions in the analysed regions have complicated forms. The results prove that the displacements, stress and strain distributions of the vertebrae arch under variable loads of spinous process is very irregular.

The experiment has proved that holographic interferometry can be used for simultaneous measurements of three components of the displacements of the examined surface. Determining the displacements allows calculating strain and stress and therefore strain or stress tensor of surface can be found.

Using the traditional holographic interferometry it is possible to elaborate a complete method to measure three components of displacements in the area of human lumbar vertebrae.

The displacements measured in three independent, not planar direction gives a complete information about the displacement. Knowing the mutual position of these directions and their orientations in relation to an arbitrary Cartesian system connected to analysed system it is possible to describe the displacements in the orthogonal xyz system [6]. In order to fully describe the displacements we need to record three holographic interferograms, each in different directions. Once it is done we can calculate displacement components in directions of sensitivity of those interferograms.

Three interferograms were recorded as three-dimensional using the scheme proposed by J.E. Solid in order to determine the spatial components of a point on the surface of the vertebra [29]. The holographic interferometry method makes it possible to simultaneously determine, without touching, displacements in the whole investigated area of the vertebra. For this purpose one

must solve a system of the following three equations:

$$\lambda N_i = \Delta x \left(\frac{x - x_{Qi}}{Q_i P} + \frac{x - x_{Ri}}{PR_i} \right) + \Delta y \left(\frac{y - y_{Qi}}{Q_i P} + \frac{y - y_{Ri}}{PR_i} \right) + \Delta z \left(\frac{z - z_{Qi}}{Q_i P} + \frac{z - z_{Ri}}{PR_i} \right), \quad (4.17)$$

where indices $i = 1, 2, 3$ denote data and results relating to three measurements.

For the recording, three holographic plates were set at different angles relative to the investigated surface of the vertebral arch and the object was illuminated by one beam. The interferograms were recorded using the double-exposure technique. The displacement of a given point on the investigated surface in the directions of sensitivity vectors proper for each of the interferograms was determined for each of the three simultaneously recorded holograms.

The values of the three displacement components along the directions of the vectors were calculated using the following relation:

$$dx_{1,2,3} = \frac{N_{1,2,3} \lambda}{2 \cos Q_{1,2,3}}. \quad (4.18)$$

The investigations were conducted under loads simulating the compression of the vertebral body and the bending of the vertebral arch (the loading of the spinous processes). An example of interferogram of the vertebral arch when the spinous process is loaded with the force increment of $4N$ is shown in Fig. 16.

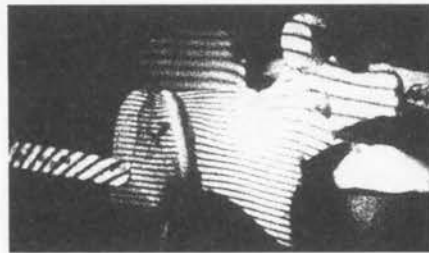


FIGURE 16. Interferogram of the vertebral arch.

Results

A diagram of the cross-section for which the values of the displacement components and then those of the strain and stress tensor components were determined are shown in Fig. 17.

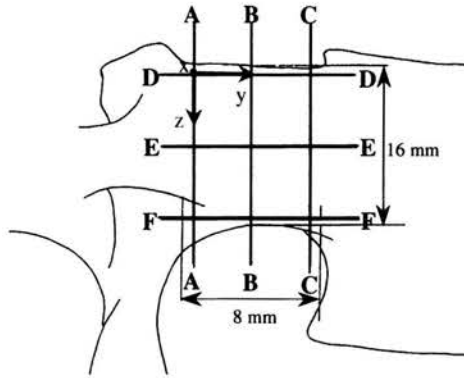
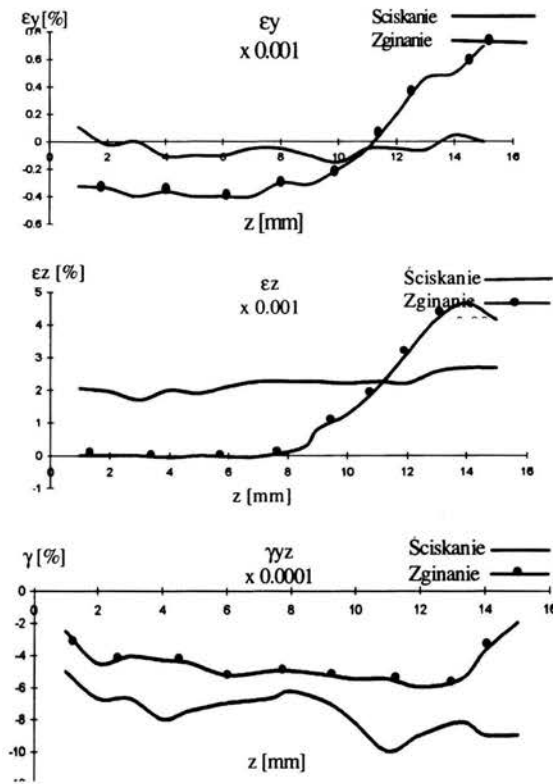


FIGURE 17. Diagram of the cross-section.

FIGURE 18. Distributions of strains ϵ_y , ϵ_z , γ_{yz} for the middle cross-section of pedicle B-B.

After interferograms of the three spatially situated holograms were recorded it became possible to determine the displacement components (dx, dy, dz) and then the strain components. When values of the material constants were assumed, the stress distributions were determined. Example of distributions of the strains $\varepsilon_y, \varepsilon_z, \gamma_{yz}$ for the middle cross-section of pedicle B-B (according to Fig. 17) are presented in Fig. 18. One of the graphs is for flexural loads acting on the spinous process (simulation of bending forward) while the other, for loads compressing the vertebral body (Fig. 14).

Conclusions

The developed research methodology involving the determination of three displacement components by means of the holographic interferometry technique makes it possible to determine very small values of displacement and stress components. The methodology can be applied to the investigation of real objects, like cadaver vertebra specimens. Three-dimensional holographic interferometry is particularly suitable for biomechanical studies since the displacement of a real object is measured and the measurement does not involve touching.

The strain and stress distributions in the vertebral arch vary significantly depending on the applied scheme of loading. Because of the complex structure of the vertebra (sharp variations in its cross-section and mechanical properties), the strain and stress distributions in the analysed regions have complicated forms.

4.7. Studies of femur bone

The hip joint [1, 4] is one of the most heavily loaded joints in the human organism and thus subject to degenerative and deforming changes. Still, thanks to the solid structure of its bone elements and the strong muscles and ligaments it is highly adapted to carrying heavy static and dynamic loads. The state of loading of the whole skeletal system of the hip joint is a resultant of the interaction between the head and the acetabulum and the tension of the muscular system. The abnormal distribution of loads, due to abnormalities in the anatomic structure of the hip joint's bone elements, may lead to hip dysplasia and rapid degenerative-deforming changes. Valuable information can be gained from a comparative analysis of the displacement of the femur bone and that of the same bone with implanted hip-joint endoprostheses.

One direction of the research conducted in our laboratory is the investigation of the effect of the rigidity of the hip-joint endoprosthesis pin on the distribution of strains in the bone. The rigidity of different endoprostheses used in clinics in Poland has been tested. This parameter is a significant

factor contributing to such negative phenomena as “remodelling” and “shielding”, i.e. the reconstitution of bone structures and the creation of zones of undeformable bone structure. These phenomena are usually connected with the rebuilding of the bone structures around the implant and they often result in the loosening of the implant or in the destruction of the bone around it [1, 4, 9, 17]. The effect of the implantation of a prosthesis on the deformation of the femur bone surface is shown in Fig. 19. A complex loading system, incorporating the action of the gluteal muscles, the hip-tibia band muscles and the rotators, was employed.

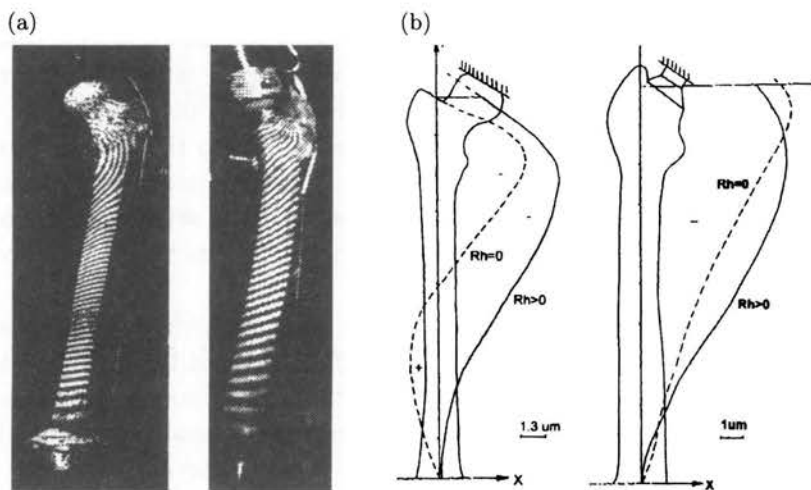


FIGURE 19. Example of fringes distribution: (a) intact femur and femur bone with non-cemented endoprosthesis (A), (b) $R_h = 0$, without rotator muscles.

4.8. Studies of the displacement of the human jaw

Fractures of the human jaw are one of the most common injuries of the facial part of cranium [37]. Various types of artificial plates have a practical application in the treatment of this injury. Type of fracture, the geometrical features of the plate and its mechanical properties decide about quality of the junction and final results of the clinical treatment.

The aim of this work was to determine the displacement and strain distribution in the human jaw before and after implantation during biting. The epoxy resin model of the jaw (Fig. 20), with simulated typical fracture was analysed using the holographic interferometry method.

Two artificial plates made of titanium alloy combined the jaw fracture. Applied load system reflected the anatomical and biomechanical conditions.

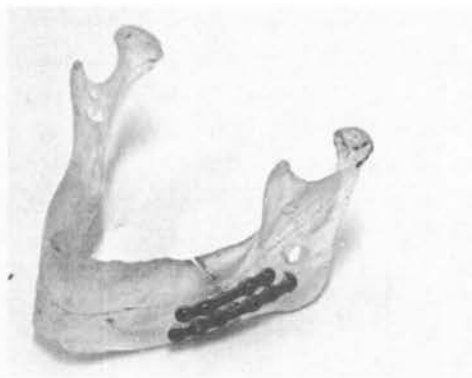


FIGURE 20. Model of the jaw with the plates.

In this particular investigations three kinds of load were considered: first force was applied onto the frontal incisors, and separately onto the left and the right canine tooth (Fig. 21).

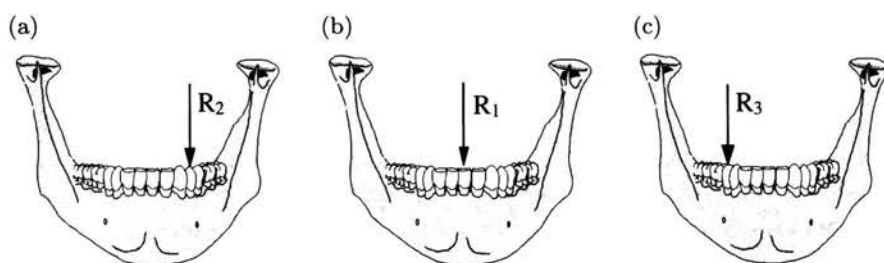


FIGURE 21. Schemes of the applied load systems.

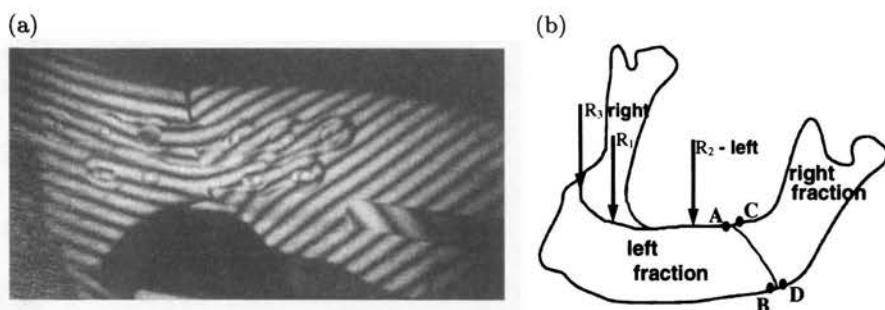


FIGURE 22. (a) An interferogram of jaw with two plates. (b) Points at the instant of the fracture in which the value of displacements were measured [37].

On the basis of series interferograms it was possible to determine the value of the displacement in the particular points (Fig. 22(b)) at the fracture boundary on the left and the right fractions of jaw.

The upper boundary of the displacements of the jaw fractions in the gap of fracture is not determined exactly. On the basis of clinical observations it is assumed that displacements of fractions could not exceed 1 mm. Obtained results show that this system of stabilisation, which is often used in clinical practise, guarantees proper stabilisation of the bone fractions.

These results can be used in future investigations to vary the geometric features of the plates.

5. Application of speckle photography

5.1. Principle of speckle photography method

Speckle photography [1, 7, 8, 11], similarly as holography, is a non-touch measurement technique and it is used to analyse displacements in a direction parallel to the surface of an object and to measure the deflection and the angular displacement of a normal to the investigated surface. This technique exploits the so-called speckle effect associated with the diffusion of coherent light by an optically nonsmooth surface. In the considered case, laser light rays while illuminating an investigated area are reflected and dissipated by the bone's surface irregularities. By interfering with one another they form a pattern of light and dark speckle situated in front of the dissipating surface. There is a close relationship between the pattern of speckles and the particular points on the surface. As the illuminated area of the bone displaces so do the particular speckles. By recording the pattern of speckles, using the double exposure technique, before and after loading a specklegram is obtained.

The main advantage of speckle photography technique is the possibility of simultaneous recording in a whole measurement field whose dimensions are limited only by technical capacities. Practically, it is possible to record displacements in the whole-investigated area during one exposure. This is particularly important if one takes into account high variability of mechanical properties of the bone and thus the variability of the distribution of its deformations and displacement of points lying on its surface. Additionally this non-contact method does not introduce errors, associated with the direct influence of the measurement path on the investigated object, into the measured quantities [17, 28, 31].

The speckle method is used for the analysis of displacements in the direction being parallel to the surface of the object. This method makes use of the so-called speckle effect connected with phenomena accompanying the coherent light diffusion through an optically irregular surface.

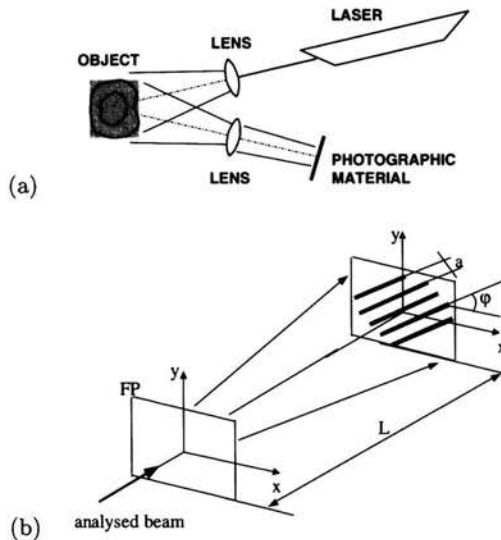


FIGURE 23. Optical arrangement for recording of specklegrams (a) and for reconstruction of the specklegram and measurement the distance between fringes and an angle of inclination φ (b) [1].

The rays of the coherent light beam illuminating the area investigated undergo reflection and diffusion on randomly spaced irregularities. While interfering mutually they form a structure of tiny, dark and light speckle located in the space before the diffusion surface. Due to the deformation of the illuminated object particular speckles undergo displacements. By recording (in the measuring system as shown in Fig. 23), the structures of the speckle corresponding to different states of the displacement of points of the surface being tested, e.g. by means of double exposure technique, one can obtain its speckle photography. It contains information on the value and direction of displacement in the plane parallel to the object. It should be pointed out that the size of the speckle formed in the space undergoes a change being visible on their photo image (after being transformed by means of the optical system):

$$\sigma = 1.22\lambda F = 1.22\lambda \frac{L}{D}, \quad (5.1)$$

where:

L – the distance of image form the lens,

D – diameter of entrance pupil,

σ – mean diameter of the image of the speckle,

F – aperture value of the lens,

λ – length of light wave.

Corresponding to the difference in the position of two images of the same speckle (before and after deformation) is the displacement in the plane of the object d^* , the distance between the points on the specklegram being equal to

$$Q = p \times d^*, \quad (5.2)$$

where p is the magnification of the mapping system.

In practice, we usually have $4L^2 \ll a^2$, and then (5.2) yields:

$$|d^*| = \frac{\lambda \times L}{p \times a}, \quad (5.3)$$

where a is the distance between the pattern of the screen.

The direction of the vector d^* is rectangular to the direction of the patterns on the screen, and thus considering their inclination angle the components of d^* are as follows:

$$u = |d^*| \sin \varphi = \frac{\lambda L}{pa} \sin \varphi, \quad (5.4)$$

$$\nu = |d^*| \cos \varphi = \frac{\lambda L}{pa} \cos \varphi. \quad (5.5)$$

Subjecting of the specklegram to overexposure with the use of a coherent light beam results in its diffusion.

5.2. Analysis of displacement of knee joint

In the case of advanced disturbance of lower limb geometry with varus deformity of the knee, total two or three-dimensional alloplasty is commonly employed as a treatment [7, 8]. If there are general or local contradictions, even in extensive arthrosis of the knee with varus position and lateral or antelateral instability, interligamentous popliteal osteotomy (Coventry) may be performed. The difference between the costs of the two solutions is also of significant importance. Clinical studies conducted for several years now at the Orthopaedic Department of the Rehabilitation Health Care Centre in Wrocław indicate that it is necessary to modify the Coventry technique. On the basis of the clinical studies and studies of knee joint biomechanics, a procedure was developed for performing popliteal osteotomy in patients in whom the shape of whole lower limb contribute to the subluxation (defined as a distance between the limb's mechanical axis and the anatomic centre

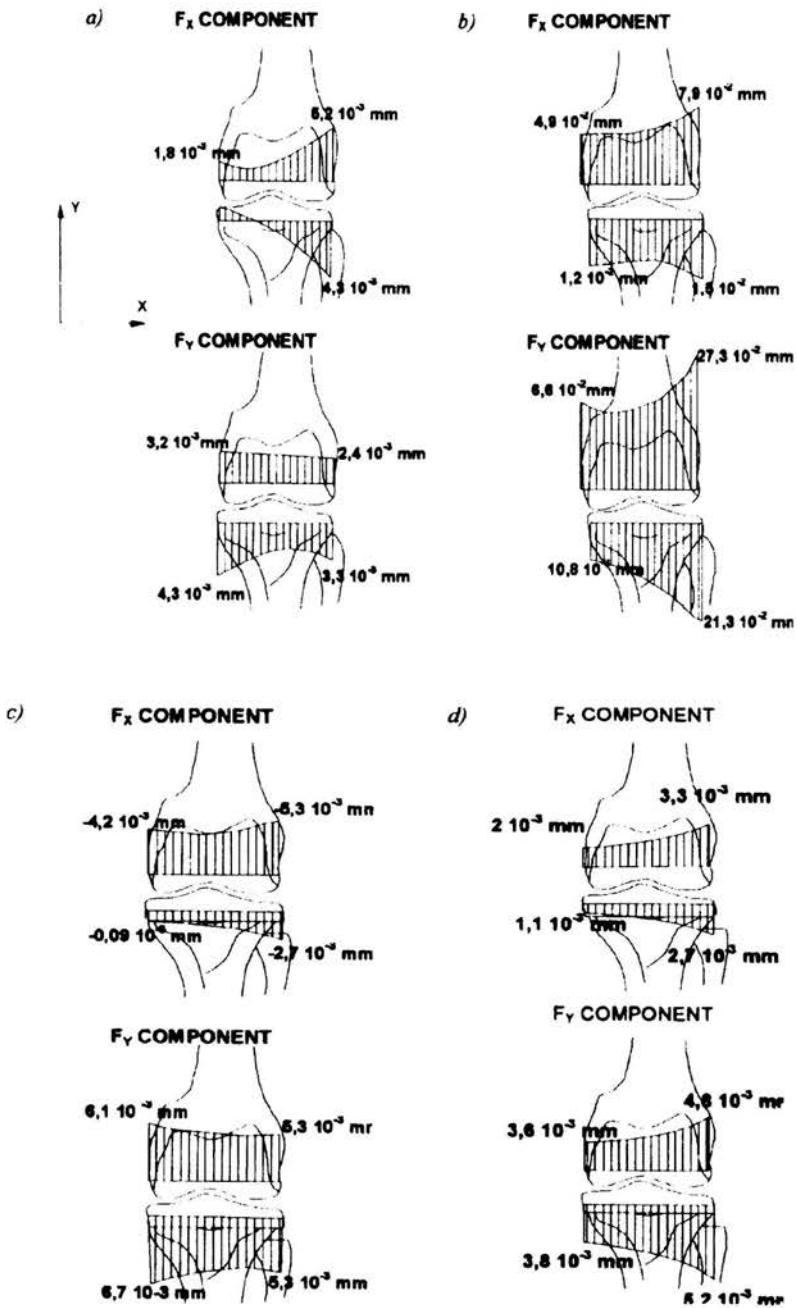


FIGURE 24. Graphs of displacements measured in coronal plane: (a) stage I, (b) stage II, (c) stage III, d) stage IV [36].

of joint at the level of the articular space) of the knee joint when the traditional operative procedure is employed. Therefore the main target of these investigations was to verify experimentally the proposed operative procedure. The investigations covered comparative studies of the knee joint in four conditions: anatomically and physiologically normal joint (stage I), varus joint (stage II), joint after Coventry popliteal osteotomy correction (stage III), and the joint after new variety of the Coventry procedure (stage IV).

In the investigations of the displacement of points on the surface of bone, the model of the knee joint was constructed from real autopsy preparations – bones dissected free and suitably prepared. The investigations were conducted only in static conditions. In the investigations, symmetric standing on the two lower limbs at full extension and asymmetric standing on one lower limb at full extension were reproduced.

The interaction between the articular surfaces was evaluated by measuring the frontal plane displacements of points lying near the articular space which was done by speckle photography. Displacements in the region of the articular space were measured along a line parallel to it. Results of the experimental investigations are shown in Fig. 24.

In stage I, displacements in the frontal plane indicated a very stable position of the knee joint. It is observed that vectors of frontal plane components of displacement on lateral condyle of tibia are directed laterally, and vectors on medial condyle of tibia are directed medially. In stage II, every displacement vector on the tibia is directed laterally – it is the effect of increasing varus deformity under applied load. In stage III, displacement vector on the tibia condyles is directed medially as a result of correction. The stage IV is similar to stage III, but increasing displacement is visible.

5.3. Analysis of displacement of hip joint

The well-known Pauwels models [8], making it possible to simplify the applied bone loading schemes, were used to analyse forces acting on the epiphysis of the proximal femur bone. A special bone loading system (Fig. 25(a)) and an optical system were designed and built for the investigations. The femur bone, positioned differently relative to the vertical axis: at 7° and 14° , was investigated. Also results obtained in the case when the gluteus and tractus iliatiobialis was taken into account and in the case when it was not taken into account were compared. Figure 25(b) shows a specklegram with a plotted lattice of points at which displacements were analysed. The results of this analysis for the displacement of the epiphysis of the proximal femur bone are presented in the form of graphs (Fig. 26) with marked schemes of loading applied at the particular stages of the investigation. The results in-

dicates that the angle of inclination of the femur bone has a significant effect on the distribution of displacement components.

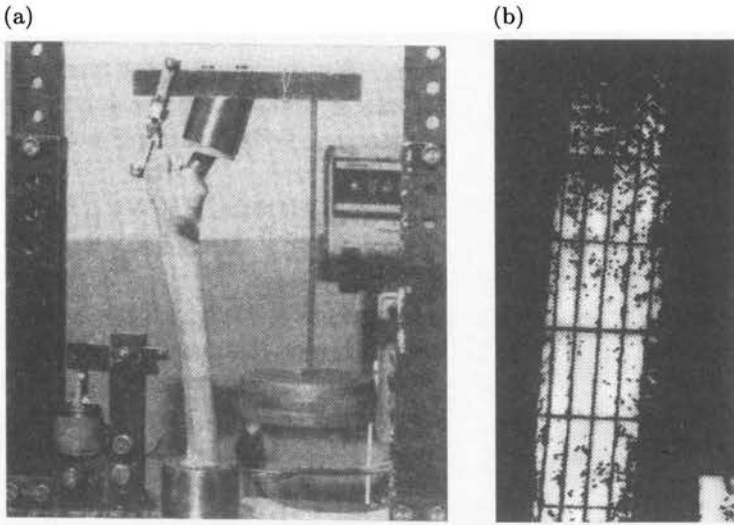


FIGURE 25. (a) The load system. (b) Example of specklegram.

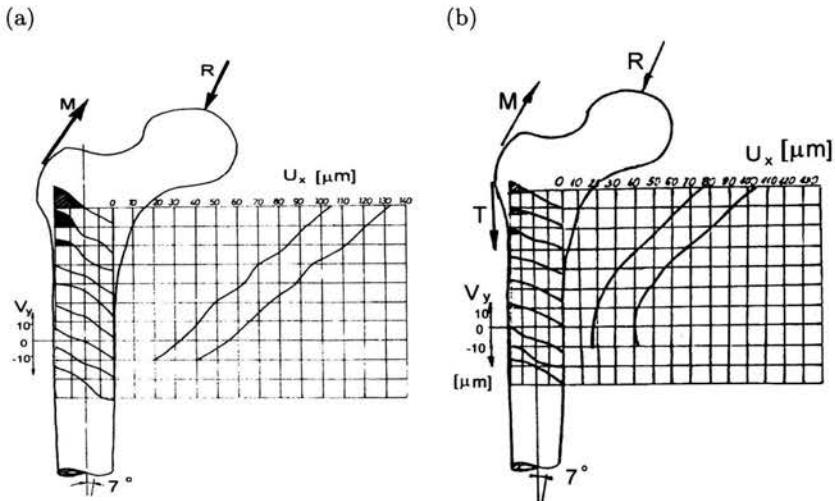


FIGURE 26. The displacement distribution in the femur bone: (a) femur position angle 7° without tractus iliaticus action, (b) femur position angle 7° with tractus iliaticus action.

6. ESPI – Electronic Speckle Pattern Interferometry

Recently significant improvements of laser Doppler techniques gained interest for bone analysis [3, 30, 31, 35]. Laser speckle interferometry ESPI allows the full field and three-dimensional measurement of deformation and strain on complex surfaces. In electronic speckle pattern interferometry (ESPI) (Fig. 27), a speckle pattern is formed by illuminating the sur-

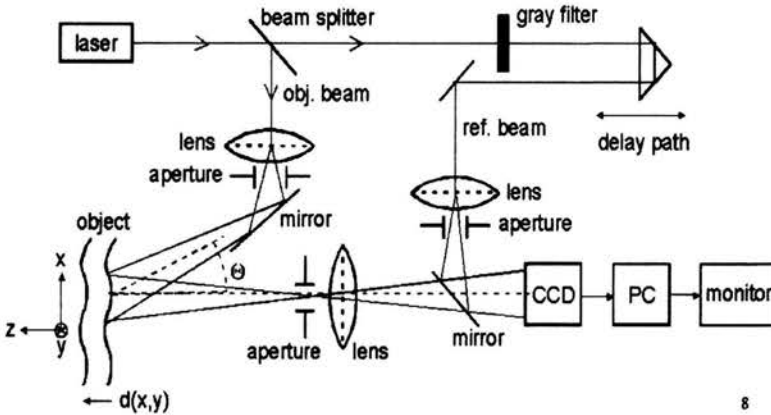


FIGURE 27. Scheme of optical set-up of the ESPI [35].

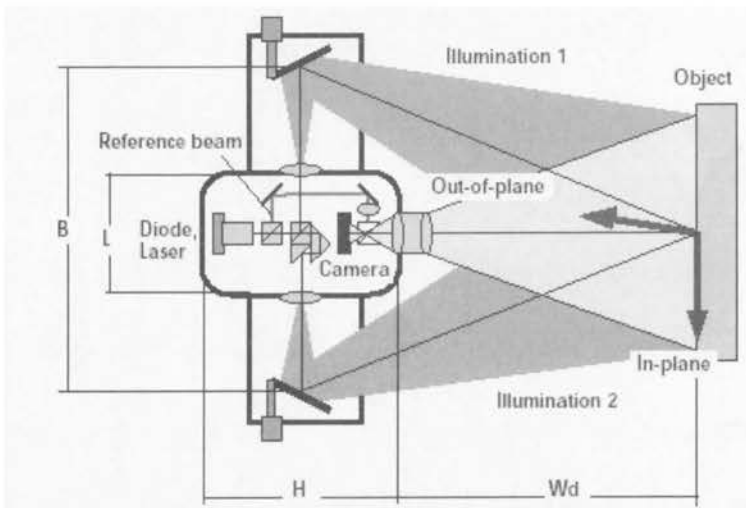


FIGURE 28. Diagram of the typical optical configuration [35].

face of the object to be tested, with laser light. This speckle pattern is imaged onto a CCD array where it is allowed to interfere with a reference wave, which may or not be speckled. The resultant speckle pattern is then transferred to a computer where it is stored in memory and displayed. When the object has been deformed, or displaced, the resultant speckle pattern changes due to the change in path difference between the wavefront from the surface and the reference wave. This second resultant speckle pattern is transferred to the computer and subtracted from, or added to, the previously stored pattern and the result is rectified.

The resulting interferogram is then displayed on the monitor as a pattern of dark and bright fringes, called correlation fringes, as the fringes are produced by correlating the intensities of the resultant speckle patterns taken before and after displacement. It is possible to continuously grab frames while a deformation is occurring and subtract them in succession from the first speckle pattern, in real-time. In this way it is possible to observe the real time formation and the progressive changes of the fringe pattern related to the deformation of the surface.

The fringe patterns obtained by the ESPI technique represent contours of equal displacements. The spacing of the fringes is inversely proportional to the displacement and, in in-plane systems, the fringes are aligned perpendicularly to the direction of the displacement. Two consecutive dark or bright fringes represent a displacement whose exact value depends on the wavelength of the light used and the geometrical set-up of the ESPI system. This value of this displacement is called the fringe sensitivity term. The displacement between two points can be easily calculated by simply counting the number of fringes between those points and multiplying by the fringe sensitivity term. This can be a slow and tedious process when analysing complex fringe patterns and there is a relatively large error associated with this technique. However, with high-speed digital computers the fringes can be quickly processed using automatic fringe analysis and precision phase measuring techniques to provide accurate quantitative results. The most common techniques for this interferogram interpretation are the Fourier transform and phase-shifting methods [35]. ESPI enables to determine the values of displacements both in vivo and in vitro conditions under different state of loading: statical or dynamical.

6.1. Application of ESPI for measurement of anisotropy mechanical properties of bone tissue

The biological structure of bone is known as very complicated, built of rods, plates and beams (called trabeculae), which create the main load car-

rying system. In order to provide a best possible stress and strain distribution throughout the whole bone, the growth of bone elements is controlled by many processes based on electrical, chemical, biological and mechanical principles. These processes are called 'physiological adaptation' (Wolff's Law) and result in an highly anisotropic architecture of bone tissue. This, on the other hand, creates difficulties as far as numerical calculation (FEA) of a joint implant (e.g. artificial hip or knee joint) is concerned, since the distribution of forces and displacements throughout the new structure should be similar to the former natural structure. It is also known that in clinical practise the parameters for describing bone tissue are radiological parameters (e.g. radiological density). We investigated the anisotropic behaviour of bone tissue and investigated (possible) relations between mechanical and radiological properties of bone.

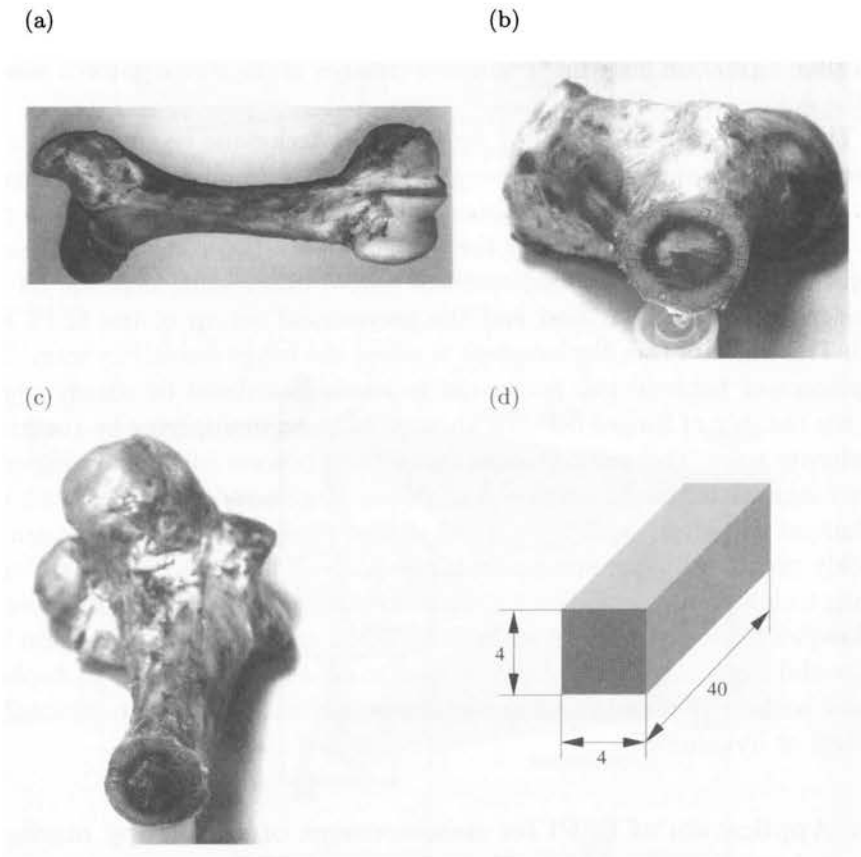


FIGURE 29. (a) Used bovine femur bone. (b) Distribution of I group samples. (c) Distribution of II group samples. (d) Bone samples.

Overall 24 samples were used, both from the diaphysis of bovine femur bone [22, 33]. 12 samples (I group) were taken from the part near to epiphysis, the other 12 samples (II group) were taken from below the region of I group samples. The distribution of the samples over the circumference as well as the preparation of each sample is shown in Fig. 29.

Sample number 1 and 2 (I and II group) were taken each from the part of circumference below great trochanter (trochanter major). The numbering of the other samples was done clockwise.

The test set up was constructed for three-point-bending of the bone samples. The construction is shown in Fig. 30.

Results were recorded by means of displacements. All samples were laid for bending test in the same manner. In the resulting images left side corre-

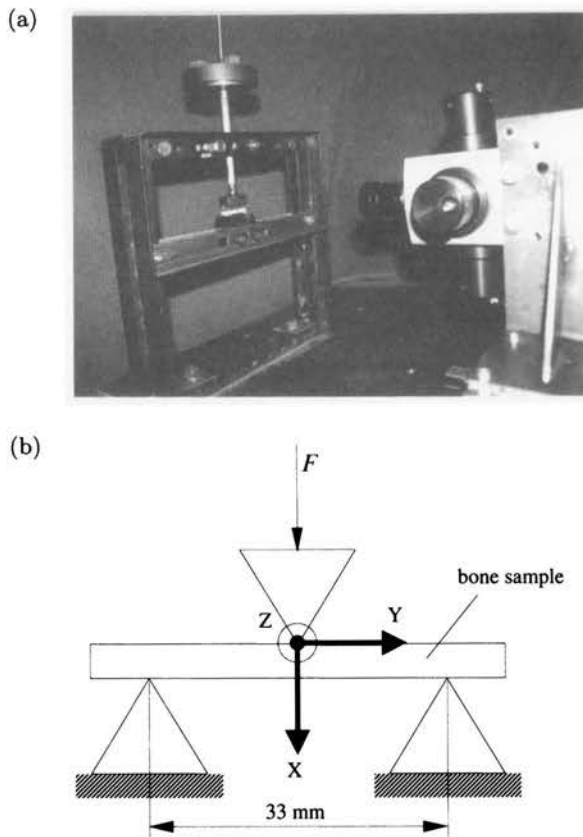


FIGURE 30. (a) Test setup with head of ESPI system. (b) Sketch and of test setup. (c) Detail of constructive design of test setup.

sponds to distal end of the sample, and right side corresponds to proximal end of the sample.

Load applied to all samples was 1089 G for preload and 300 G for actual load. This section contains only example result obtained for t-sample number 9. Figure 31 shows displacements in all of three directions and arrow representation of the displacement. The arrow representation indicates in-plane displacement vectors; background is out-of-plane displacement.

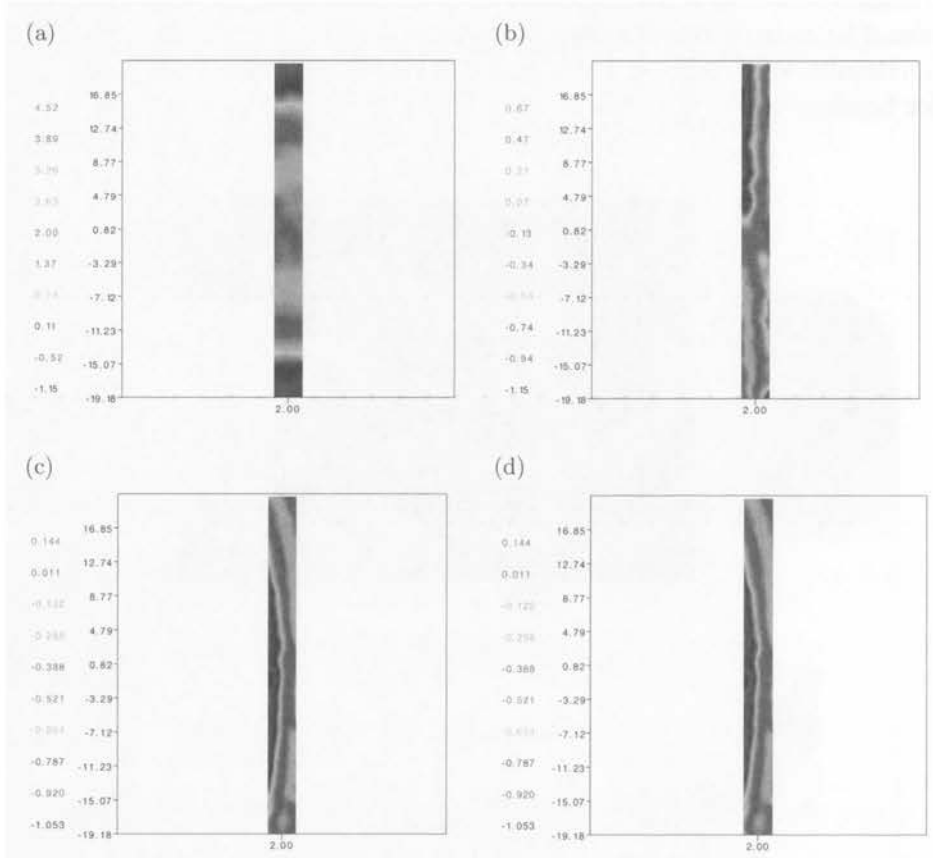


FIGURE 31. Result displacement of sample t-9 side A load on surface B: (a) displacement in the x direction, (b) displacement in the y direction, (c) displacement in the z direction, (d) arrow representation of displacement.

Examples of results are shown in the following figures. The deflection in the x -direction can be used for calculation of the elastic modulus. Figure 32 contains graphs of distribution of the elastic modulus calculated using the

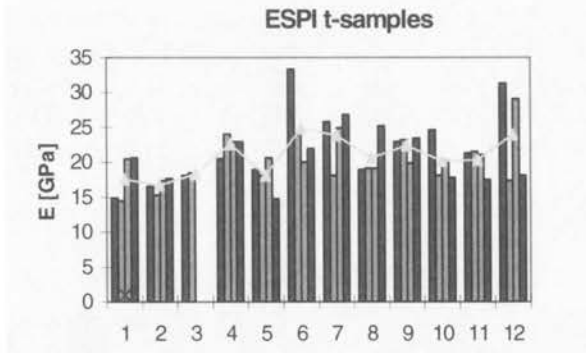


FIGURE 32. The elastic modulus calculated for each side of each t-sample. Yellow line indicates the mean value of the elastic modulus for a single sample (averaged over four sides).

formula:

$$E = \frac{Fl^3}{4b^4y_m}, \quad (6.1)$$

where $F = 0.3 \cdot 9.81 = 2.94 \text{ N}$, $l = 33 \text{ mm}$, $b = 4 \text{ mm}$, and y_m is the measured deflection.

We note that accuracy of ESPI measurements is high enough to be sure that the differences of obtained results are independent of measurement system. It was checked, however, in repeatability test. Possible explanations can be found in loading system and bone itself. However, explicit differences were found between results obtained with ESPI and additional investigations carried out using testing machine.

However, the nature of both methods is different. In the case of ESPI, the resulting elastic modulus is calculated from a single measurement taking deflection of chosen point. In the case of testing machine, the resulting elastic modulus is calculated from a series of measurements. Thus, the ESPI measurements are more sensitive to environmental factors. Whereas the loading system was similar (two supporters in the same distance and beam loaded in the middle point), the load was different. With the ESPI a preload is necessary to stabilize the system. Displacement resulting from additional load is measured. However, practice showed that the preload used was insufficient. This insufficiency was imposed by the requirement of staying in the elastic region. The elastic region was determined after machine testing in destructive bending. Thus, the preload stayed underestimated.

Testing machine loads the beam with constant rate cancelling possible inaccuracies of load application that are unavoidable with the loading system applied with ESPI measurements.

Considering mean values of the Young modulus averaged over A, B, C, and D sides of t- and d-samples (presented in Fig. 33) it can be concluded that the ESPI results have lower values compared to MTS results.

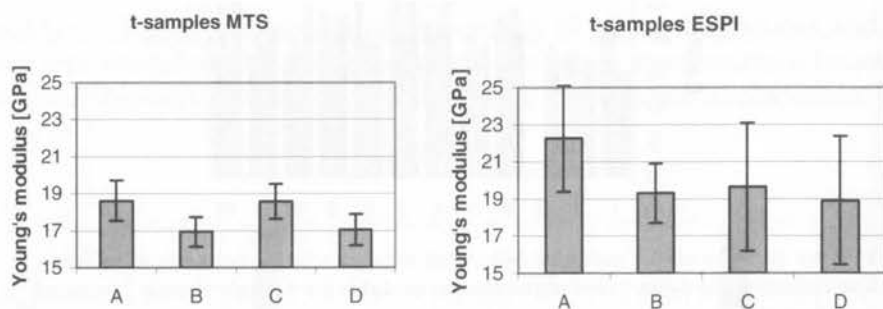


FIGURE 33. Mean values of elastic module averaged over sides A, B, C and D with standard dispersion as error bars.

Furthermore, the standard dispersion of the ESPI results is far greater than the equivalent MTS results. An explanation has been provided above. Differences in load application and viscoelastic properties of bone seem to be the most affecting. Constant rate of bone load results in distinct deflection than discrete loading with random rate. However, the observation of similarities in Young's modulus for opposite sides and differences in Young's modulus for adjacent sides is valid for both methods.

Nevertheless, the ESPI was found peculiarly suitable for strain field determination, simultaneously in three dimensions. This feature is exclusive for the ESPI. Furthermore, it gave an insight into structure-strain relationship far more detailed than it is possible with techniques known so far. Especially, when small specimens are considered.

To recapitulate, the bovine compact bone of the femur was shown to be more tough in circumference than in radial direction. This is surprising. It has been known from strength of materials that pressure applied to hollow shaft (similar to long bone) results in stress at circumference twice as big as in radial direction. Therefore, bone seems to adapt its structure to loading environment.

Considering the distribution of Young's modulus at circumference at both levels (trochanter and diaphyseal), no conclusion can be stated until muscle attachments are taken into account. Samples cut near trochanter (t-1, t-2, t-3, t-12) exhibit lower Young's modulus. According to muscle attachments, that is the region where no muscle are attached. Thus, the bone underlying this region undergoes relatively lower loading. For corresponding d-samples this relation is not as strong as for t-samples since in the region where d-

Investigations of displacement distribution of human pelvis bone using the ESPI method were carried out [27]. The main aim of these investigations was estimation of behaviour of normal pelvis bone, pelvis with degenerative changes of shape around acetabulum, and after surgical correction (alloplasty). Basis of this analysis is estimation of changes in strain distribution under applied loads, especially in the region of acetabulum.

Special load set-up was designed for testing (Fig. 35), which allows realising load apply according to basic models of hip joint load.

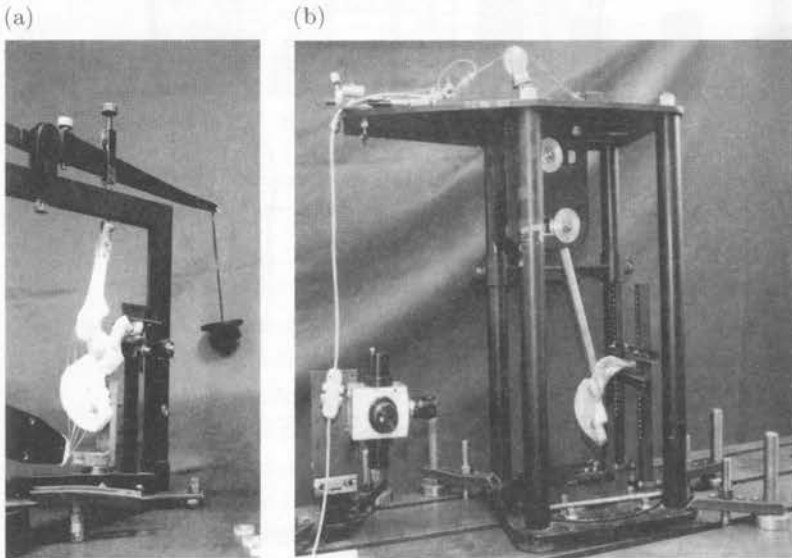


FIGURE 35. (a) Load setup used in pelvis bone investigations. (b) Investigated surface of pelvis bone.

An example of phase map recorded in measurement process is shown in Fig. 36.

Recorded distributions of displacement of pelvis bone show that applied load results in complex state of displacement, strain and stress distribution.

Main part of bone moves laterally as a result of acting of applied hip joint reaction. Line of this acting force is shifted laterally according to fixation in pelvis-sacral joint.

In this region main part of all bone mass is concentrated, also geometrical dimensions of bone are highest. Because of that the vertical displacements are relatively small. Going to the lateral part we can observe increasing of vertical displacements. It allows to conclude that pelvis bone is bonded laterally, and the main part of bone rotates around fixation point. In the region of pelvis-sacral joint we can observe large disturbance of displacements distribution

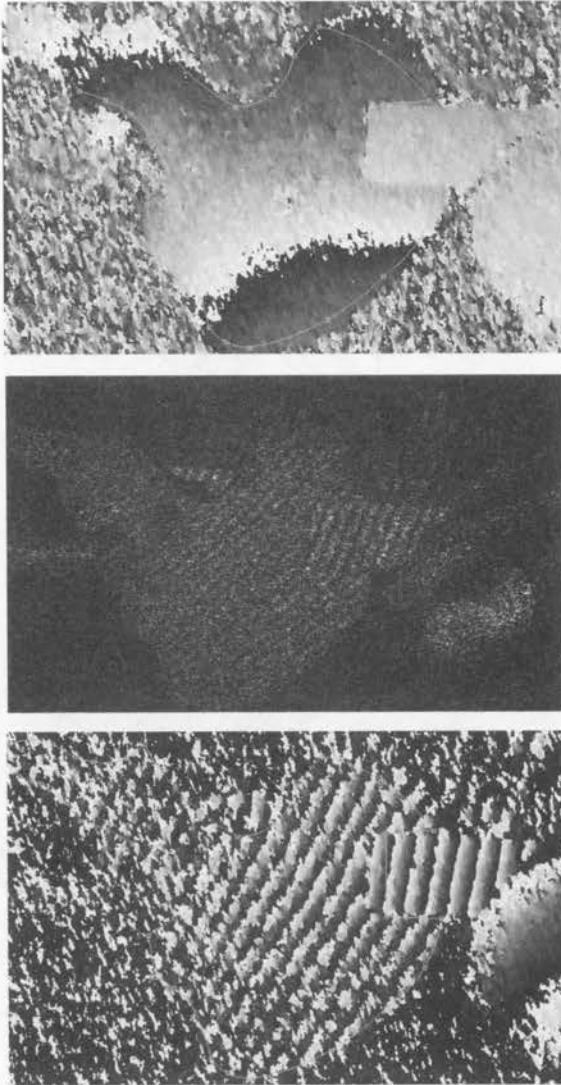


FIGURE 36. An example of phase maps recorded during measurements.

as a result of fixation. The medial part of pelvis bone moves medially and downwards. This situation is similar to rotation of main part of bone, but this rotation around acetabulum region is a result of deformation of acetabulum.

Also, some rotation effect can be observed in saggital plane. Recorded results are basis of estimation of phenomena connected to bone tissue remodelling and are a good example of boundary conditions for finite element models calculations.

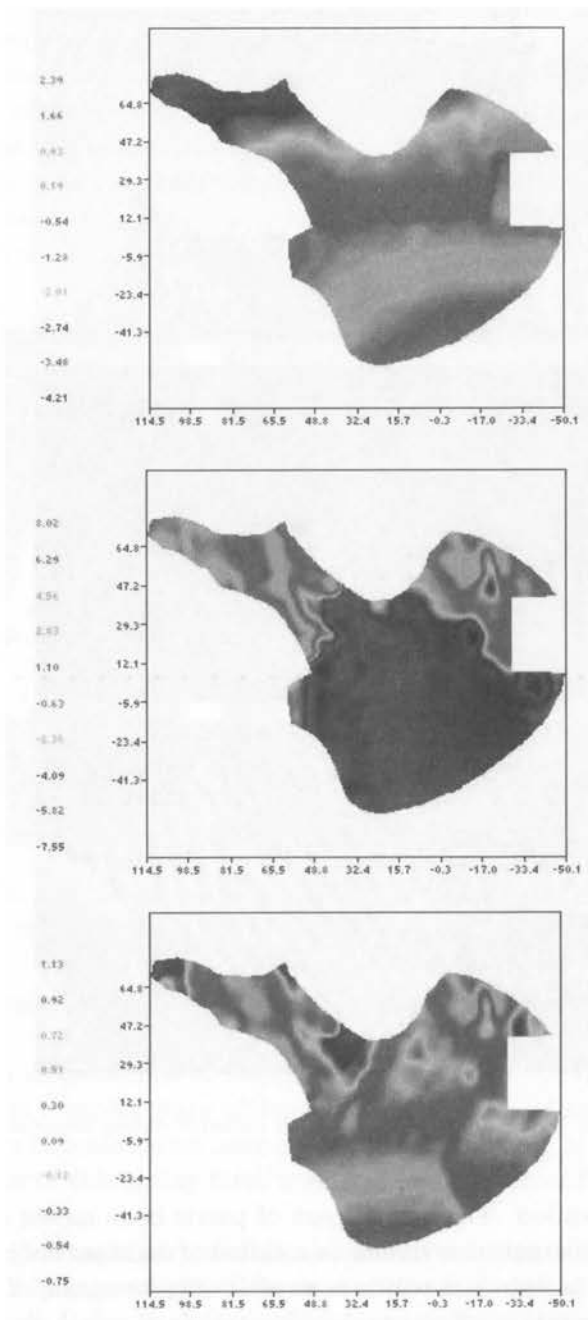


FIGURE 37. An example of displacement distribution along x , y and z axis.

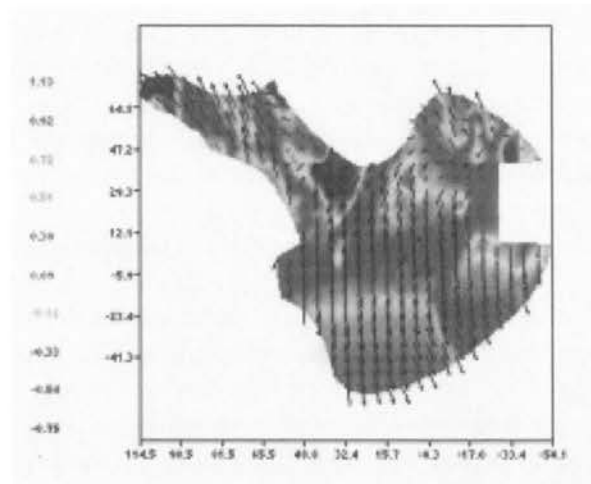


FIGURE 38. Visualisation of displacement distribution.

7. Application of strain gauges

Extensometry [1, 5, 17, 21] deals with methods of measuring deformations of solids. Changes in the length of segments of straight lines connecting points on a body and changes in the angles between the segments reflect the deformations of the solid. Extensometers are instruments which exploit the phenomenon that the resistance of the conductor changes as it expands or contracts. They are precision instruments characterised by high sensitivity, a slight measuring error and measurement repeatability. Extensometers which are used to investigate stresses and strains in structural elements can be divided into two groups: electric extensometers and mechanical extensometers. An appropriate type of an extensometer is selected depending on the measurement conditions and requirements associated with the kind of a material, the shape of a structural element and the kind of loading.

7.1. Experimental analysis of external fixator for femoral bone elongation

The interest in the external fixation system for limbs developed by Ilizarov has been growing in the last decade [1, 5, 18]. This is above all due to the high, in comparison with other fixators, effectiveness of treatment by the Ilizarov fixator of, e.g. complicated fractures of long bones, pseudarthrosis and limb axis correction or shortening. This high efficacy of the Ilizarov fixator results from, among others, its modular design that allows one to create numerous configurations of the fixator and to modify its spatial arrangement during

treatment depending on the needs. Another advantage is that the mechanical properties of the fixator are conducive to the preservation of the optimal biomechanical conditions at the place of the joint of the bone fragments. The Ilizarov fixator is a flexible stabilizer. This means that the load acting on the bone are carried both by the structure of the fixator and fragments of fractured bone, ensuring the axial dynamisation.

The elongation of the lower limbs is one of the more interesting, but highly complex, both in the clinical and mechanical aspects, cases of the application of the Ilizarov fixator. Though the clinical experience in the elongation of the lower extremities by means of the Ilizarov fixator is long, many disturbances and complications still frequently beset this process. This is particularly the case when the lower limbs are elongated in the thigh sections where complex conditions of a load acting on the femoral bone in the hip joint occur in usually strongly developed muscles groups surrounding the thigh subject to distraction. The failures in the distraction are above all due to still unexplained mechanisms of the effect of the fixator on the limb begin distracted and, conversely the effect of the soft tissue surrounding the treated bone on the structure of the fixator.

Let us proceed to the analysis of the stability of the system formed by the Ilizarov fixator and the thigh being distracted [18]. The goal of such study is to determine conditions of the load acting on the particular distance rods of the Ilizarov fixator and its changes during the distraction of the lower limb in the thigh section. The tests were performed in the distance rods of the stabilizer mounted on patients undergoing thigh distraction in clinical conditions. The forces were measured in all distance rods connecting the rings between which the bone shaft was cut. It was presumed that knowing the load pattern for the particular rods and their distribution around the bone being elongated, it would be possible to determine which groups of muscles acted stronger and which weaker on the system: the bone fragments – the Ilizarov fixator and how these actions change during the whole process of distraction.

Specially adapted extensometer converters built into the distance rods of fixator mounted on patients undergoing thigh distraction were used for the measurement of the forces acting in the distance rods (Fig. 39).

The measurement covered ten cases of thigh elongation by the Ilizarov fixator. Measurements were made once a day at a fixed instant, immediately before and after the application of a distance rod length increment.

Figure 40 shows typical variations in distance rod load as a function of time recorded for selected cases. The analysis of the results recorded for the particular case shows that in most of them, the increments of forces in neighbouring rods were similar both in their character and in the variation

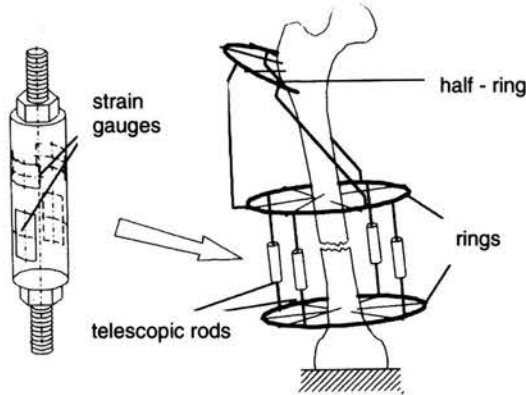


FIGURE 39. Force transducers and their localisation in distance rods of external fixator [7, 18].

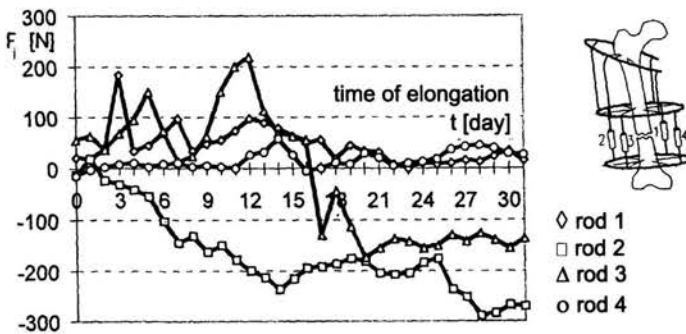


FIGURE 40. Distraction load measured in function of time; The rate of elongation: 4×0.25 mm per day [7].

of their values. The investigations have demonstrated that the stability of the system: the Ilizarov fixator – the thigh being distracted, measured in values of the transverse displacements of the bone fragments, is a function of both the mechanical properties of the adopted fixator structure and the distribution of the forces acting on this system.

The clinical studies allowed determining the distribution of loads in the particular distance rods of the Ilizarov fixator and the variation of the loads as a function of the distraction time. The clinically developed and applied measuring method allows once to control continuously the correctness of the course of the elongation of the limb by analysing the conditions of the loading of the particular rods of the Ilizarov fixator and the changes of these loads as a function of the elongation time.

The studies conducted under clinical conditions have indicated that the preliminary assessment of the physical condition of the patient, above all the degree to which the muscles surrounding the bone to be elongated are developed and trained, whether scars and pathological changes are present, is of major importance. The mechanical properties of soft tissue play an important role. The effect of optimal spatial configuration of the fixator can be selected for the particular course of treatment. This means that in clinical practice the adopted goal will be achieved in the shortest time without complications.

7.2. Analysis of strains in pelvis bone

The pelvis bone [2, 27] is a basic element of the hip joint. Human locomotor abilities are determined by the proper shape of this bone and the way in which it is loaded. The complicated and irregular geometric structure of the pelvis bone makes it remarkably fit to carry the very heavy loads resulting from the forces acting on the joint and from the body forces. The main task of the pelvis bone in the interaction with the head of the femur bone [1] is to transmit the load from the upper parts of the body to the lower limbs. The proper structure of the acetabulum is a precondition for the proper shape of the femoral head, and vice versa.

Let us now briefly discuss the interaction between the bone elements of the hip joint and the character and values of strains in the pelvis bone. Tests were carried out on a cadaver pelvis bone using the strain gauges method

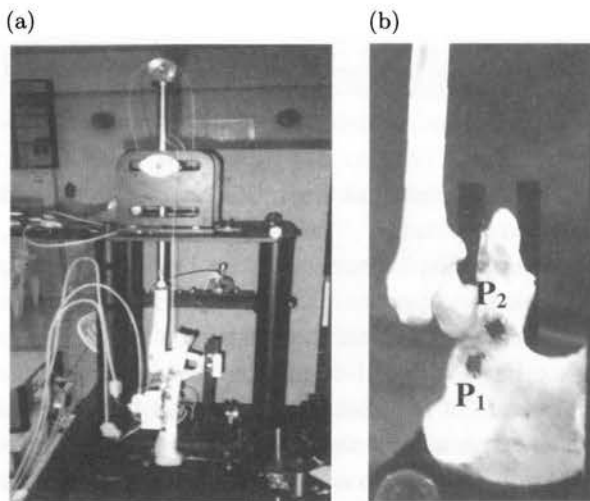


FIGURE 41. (a) Load system. (b) Location of strain rosettes.

which enables the measurement of strains under variable load conditions. Two symmetrical star strain rosettes were stuck on the bone surface close to the hip joint acetabulum in marked off areas P_1 and P_2 (Fig. 41(b)). The bone was clamped with metal angle plates in the region of its natural articular surfaces in a specially built loading stand (Fig. 41(a)). Two cases of interaction between the femoral head and the pelvis were investigated. The first case represented the proper alignment of the head whereas in the second case the femoral head was displaced to the front upper edge of the acetabulum.

An analysis of the obtained results showed that the interaction between the bone elements of the hip joint affects the character and values of strains in the pelvis bone. Higher strain values were recorded for the modelled protrusion of the femoral head from the acetabulum. The results were used to optimise the boundary conditions of a numerical pelvis bone model.

8. Application of Moiré method

It is well known that optical non-destructive testing methods have high sensitivity and they allow a full-field analysis of the investigated area without any need for physical contact with the surface. They can sometimes provide information where other experimental techniques fail or can not be applied [1, 36].

In general the term moiré denotes a regular pattern in the form of a series of parallel or crossed lines (Fig. 42) [36]. In optics the effect arises when two

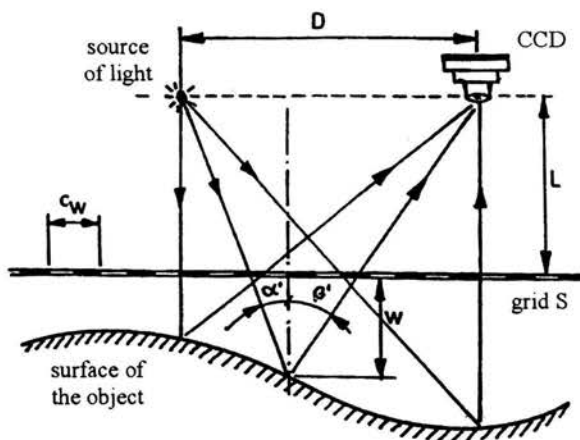


FIGURE 42. Typical configuration of the measurement system.

gratings or grids are placed in proximity with one another with a small angle between grating lines. The resulting pattern has a lower spatial frequency than those of the individual gratings, the exact value depending on the angle between the lines of two gratings.

The non-destructive testing methods, which enable to estimate the faults in posture and spine diseases, have been searched in medical diagnostic recently. The Moiré method is optical, incoherent technique, used in the analysis of the displacement field or the shape investigations and it turns out to be one of the best in this particular case. It allows to determine the shape of the human body and measure in-plane displacements of the back surface (Fig. 43).

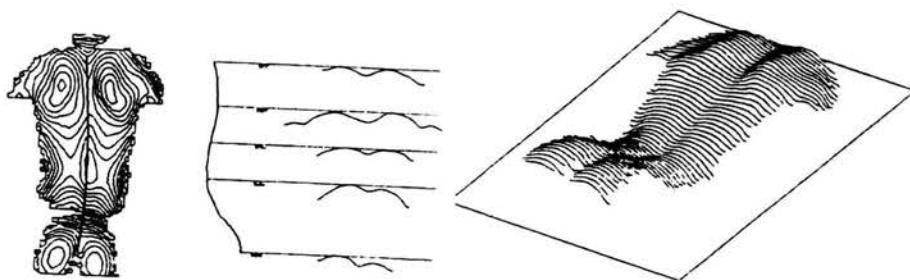


FIGURE 43. Graphical presentation of the results of deformations of the muscle-skeletal system in the human back [36].

9. Final remarks

The experimental methods, which are often used in the analysis of the displacements and the stress distribution of elements of human body, have an established position in biomechanical investigations. Currently, the biomechanical studies are carried out in many research centres all over the world, in order to explain orthopaedics diseases and work out the optimal method in treatment of human skeletal system. Investigations performed frequently concern one of the most loaded elements in human body like spine, hip joint and lower extremities. The experimental and numerical studies are mainly carried out at models and in the clinical conditions. The results of these investigations help to explain and understand both the formations of the degeneration changes in the skeletal system and elaborate efficient treatment methods.

Choice of suitable methods enabling to achieve the goal of investigations is the most important target in biomechanical studies. Physical and numerical models should both represent original models and enable to estimate

the influence of simplifications on the final results. Usually in such a kind of research it's impossible to reflect the complexity of muscle – ligament system, nervous system, biological and biomechanical factors which are inherent in skeletal – joint system of human body. Even investigations, which are carried out on specimens, also impose certain limitations. In anatomical specimen one of the most important limitation is time from sampling to testing. As it was mentioned above, the results of the experimental studies aim at verification of theoretical models. Besides that, such results can confirm and complete clinical observations. It couldn't be possible to determine the patomechanism of formation of some diseases and estimation of applied treatment method, e.g. implantation without the experimental and numerical investigations.

The experimenter when conducting biomechanical investigations, particularly of human structures, should take into consideration several factors:

1. Measurement repeatability – it is often the case that experiments are thought to have been carried out in identical conditions but the obtained results differ significantly. The measurement repeatability often depends on the precision with which the measuring points are located and on the arrangement of the directions and points of application of loads.
2. When investigating tissue structures one may encounter some problems associated with the material properties of tested element:
 - the maintenance of constant and repeatable properties of specimens,
 - the effect of temperature and hydration on the physical properties of tissues,
 - phenomena dependent on the duration of loading, such as creep.
3. Human factors such as the preparation of the experimenter (biomechanical engineer, physician) for the investigations and his knowledge of the anatomical and physical properties of the investigated tissue structures.
4. Repeatability of measurements, i.e. obtaining similar results in the same conditions replicated in other laboratories.

References

1. BĘDZIŃSKI R., *Biomechanical Engineering – Selected Problems* (in Polish), Oficyna Wydawnicza Politechniki Wrocławskiej 1997.
2. BĘDZIŃSKI R., Application of the numerical method in biomechanics, *Proc. CMM-2003 – Computer Methods in Mechanics – Gliwice 2003*.

3. BĘDZIŃSKI R., Application of the optical methods in experimental analysis of stress, strain and displacements, *Course on "Design for Quality"*, Bologna-Forli 1995.
4. BERNAKIEWICZ M., BĘDZIŃSKI R., Stress analysis in the human femur with different types of stems of the total hip endoprosthesis, in: D. Miklavcic et al. (Eds.), *Proceedings 9th International Conference on Mechanics in Medicine and Biology*, pp.543-546, Ljubljana 1996.
5. BĘDZIŃSKI R., FILIPIAK J., Experimental analysis of external fixators for femoral bone elongation, *Acta of Bioengineering and Biomechanics*, Vol.1, No.2, pp.93-105, 1999.
6. BĘDZIŃSKI R., OWCZAREK A., PEZOWICZ C., A study of the vertebral by holographic interferometry methods, *Medical and Biological Engineering EMBEC'99*, Vol.37, Sup.2, pp.256-257, 1999.
7. BĘDZIŃSKI R., ŚCIGALA K., Experimental analysis of surgically corrected knee joint, *Strain*, November 1998.
8. BĘDZIŃSKI R., SIEMASZ M., SĘPNIEWSKI Z., WALL A., Badania modelowe przemieszczeń nasady bliższej kości udowej, in: *Biomechanika'94*, Prace Naukowe IKiEM Politechniki Wrocławskiej, No.75, Wrocław 1994.
9. BĘDZIŃSKI R., TYNDYK M., Experimental methods of stress and strain analysis in orthopaedic biomechanics, *Acta of Bioengineering and Biomechanics*, Vol.2, No.2, 2000.
10. BLACHTER S., SHELTON J.C., Quantitative holographic interferometry for the analysis of surface strains in femur, Paper 1301, *Applied Optics and Optoelectronics, EOSAM'94*, pp.63-66, 1994.
11. BOONE P.M., Some coherent-optical deformation measurement techniques useful in biomechanics, in: E.G. Little (Ed.), *Experimental Mechanics. Technology Transfer between High Technique Engineering and Biomechanics*, pp.409-421, Elsevier, Amsterdam 1992.
12. BORBAS L., Elements of experimental stress analysis, *Course on "Design for Quality"*, Bologna-Forli 1995.
13. CORBY T.W., Diagnosing stress problems with photoelastic testing, in: E.G. Little (Ed.), *Experimental Mechanics Technology Transfer between High Technique Engineering and Biomechanics*, pp.455-466, Elsevier, Amsterdam 1992.
14. CRISTOFOLINI L., CAPPELO A., TONI A., Experimental errors in the applications of the photoelastic coating on human femur with uncemented hip stems, *Strain*, pp.95-101, August 1994.
15. DRAGAN SZ., WALL A., BĘDZIŃSKI R., JANKOWSKI L., Zastosowanie interferometrii holograficznej w doświadczalnej analizie mikroruchów trzpieni endoprotez bezcementowych, in: *Biomechanika'94*, Prace Naukowe IKiEM Politechniki Wrocławskiej, No.75, pp.77-81, Wrocław 1994.
16. DRAGONI E., ANDRISANO A. O., BERTUZZI F., Stress in ceramic prosthetic heads under axisymmetric loading: Effect of gaper friction, support conditions and spigot of elasticity, in: E.G. Little (Ed.), *Experimental Mechanics Technology Transfer between High Technique Engineering and Biomechanics*, pp.23-34, Elsevier, Amsterdam 1992.

17. DALLY J. W., RILEY W.F., *Experimental Stress Analysis*, McGraw – Hill, New York, 1991.
18. ILIZAROV G.A., Clinical application of the tension – stress effect for limb lengthening, *Clinical Orthopaedics and Related Research*, Vol.250, pp.8-26, 1990.
19. KAPKOWSKI J., *Basis of the Experimental Strain and Stress Analysis* (in Polish), Oficyna Wydawnicza Politechniki Warszawskiej, 1996.
20. KAPKOWSKI J., KUJAWIŃSKA M., A new hybrid technique for photoelastic investigation, *Proceedings of 10th International Conference on Experimental Mechanics, Lisbon 1994*, pp.27-30.
21. MORECKI A., *Role of the identification in experimental investigations*, Zeszyty Naukowe Politechniki Śląskiej, Seria Mechanika, Z.112, pp.125-131, Gliwice 1999.
22. MILES A.W., MCNAMEE P.B., Strain gauge and photoelastic evaluation of the load transfer in the pelvis in total hip replacement: the effect of the position of the axis of rotation, *Journal of Engineering in Medicine*, 1989.
23. ORŁOŚ A., *Experimental Analysis Strain and Stress* (in Polish), PWN, Warszawa 1975.
24. PAUWELS F., *Biomechanics in Locomotors Apparatus*, Springer-Verlag, 1980.
25. PRENDERGAST P.J., *Biomechanical Techniques for Pre-clinical Testing of Prostheses and Implants*, Lecture Notes 2, Centre of Excellence for Advanced Materials and Structures, IFTR-PAS, Warsaw 2001.
26. PRENDERGAST P.J., Finite element models in tissue mechanics and orthopaedic implant design, *Clinical Biomechanics*, Vol.12, No.6., pp.343-366, 1997.
27. PILARSKI W., BĘDZIŃSKI R., JOHN A., GAWIN E., Application of ESPI method for displacement analysis of cadaver human pelvis, *Proc. 19th Danubia-Adria Symp. on Experimental Methods in Solid Mechanics*, pp.46-47.
28. RASTOGI P.K., *Optical Measurement Techniques and Applications*, Artech House, Boston 1997.
29. SOLID J.E., Holographic interferometry applied to measurements at small static displacements at diffusely reflecting surface, *Applied Optics*, Vol.8, No.8, 1969.
30. SCIGAŁA K., *Badania modelowe charakterystyk odkształceniowych stawu kolanowego*, Ph.D. Thesis, Wrocław University of Technology, 2002.
31. STUPNICKI J., Trends of experimental mechanics, *Journal of Theoretical and Applied Mechanics*, Vol.34, No.2, pp.207-233, Warszawa 1996.
32. STUPNICKI J., Nowe obszary zastosowań i nowe metody eksperymentalne w dziedzinie mechaniki ciała stałego, *Mat. XXXVII Sympozjum Modelowanie w Mechanice*, pp.279-283, 1999.
33. STEMPNIEWICZ M., BĘDZIŃSKI R., GAWIN E., Application of electronic speckle interferometry for anisotropic mechanical behaviour of bone, *Experimental Mechanics*, 2002 (in press).
34. TYNDYK M., KRZEMIŃSKI M., BĘDZIŃSKI R., Badanie oddziaływania głowy kości udowej na miednicę, *Materiały Konferencyjne "Biomechanics – Modelling"*, Łódź 1999.

35. WEGNER R., ETTEMEYER A., Fast stress and strain analysis with microstar, *Ettemeyer Application Report*, No.05-98, 2000.
36. ZAWIESKA D., Technika mory w diagnostyce i kontroli leczenia chorób kręgosłupa, *Mat. XV Sympozjum Mechaniki Eksperymentalnej, Jachranka 1992*, pp.252-255.
37. ZIĘBOWICZ A., PEZOWICZ C., MARCINIAK J., Biomechanical stability analysis in the plate niting of mandible, *Proceedings of the 4th Polish Scientific Conference "Biomechanics '99"*, Oficyna Wydawnicza Politechniki Wrocławskiej, Vol.1, Supplement 1, pp.599-602, 1999.

